IMPERIAL COLLEGE LONDON

Department of Earth Science and Engineering

Centre for Petroleum Studies

Field measurements of spontaneous potential (SP) for smart well monitoring and control. A field test in the UK chalk aquifer.

By

Armando Esquivel García

A report submitted in partial fulfillment of the requirements for the MSc and/or the DIC.

September 2013

DECLARATION OF OWN WORK

I declare that this thesis: "Field measurements of spontaneous potential (SP) for smart well monitoring and control. A field test in the UK chalk aquifer" is entirely my own work and that where any material could be construed as the work of others, it is fully cited and referenced, and/or with appropriate acknowledgement given.

Signature: .....

Name of student: Armando Esquivel

Name of supervisors: Professor Matthew D. Jackson
Professor Adrian P. Butler
Dr. Jan Vinogradov
Donald John McAllister

Abstract

Spontaneous potential (SP) has been extensively used since the early days of oilfield exploration for identification of permeable zones and formation water salinity. However, recently SP has being finding a place in new proposed applications, e.g. monitor waterfront towards producing well during flooding operations and monitor seawater intrusion in fresh water aquifers in coastal areas. For oilfield reservoirs, the possibility of monitoring the waterfront towards the production well during flooding operations will help to implement a control system which will prevent or regulate the water breakthrough. This document presents the results of the field experiments for the electrokinetic (EK) and electrochemical (EC) components of SP in chalk aquifer in the Bottom Barn Abstraction (BBA) in Berkshire UK. The electrokinetic results were obtained during pumping conditions yielding a coupling coefficient of -97 ± 40 mV Mpa-1 which is consistent, in the error range, with the value of -60 ± 13 mV Mpa-1 obtained in laboratory tests. The electrochemical experiment consisted of the injection of brine with a concentration near a third of the salinity of the seawater. Four salt dumps were held in four consecutive days. A voltage response was measured for the first two salt dumps, later related to a redox potential response due to the metallic completion in the dump borehole in contact with the water top. Further dumps were done in plastic casing with no evidence of voltage response (i.e. EC response). The conductivity profiles may provide a link with the EC experiment results, suggesting that the concentration might have settled in the matrix or diffuse through the fracture network, thus the brine was rapidly dispersed and did not reach the monitoring wells. The result of the EK experiment confirms the possibility of monitoring the groundwater flow in field conditions to control and prevent water encroachment from injected water during waterflooding operations in oilfields. Instead, NaCl mass poured into the borehole should be increased to produce a measurable EC signal. This will replicate real conditions when seawater encroaches onto an abstraction well or is injected into a borehole in a producing oilfield as part of waterflooding operations.

Acknowledgements

I would like to express my thankfulness to my supervisor, Professor Matthew D. Jackson for his encouragement throughout the entire process and his integrity on assisting this project in all of the stages, including the field work.

I also would like to thank Professor Adrian P. Butler whose vast experience and knowledge was of especial importance to complete this document.

I am also profoundly grateful with Dr. Jan Vinogradov, at Imperial College London for his expert advice, infinite patience and knowledge shared.

Especial thanks to PhD student Donald John MacAllister, who shared his knowledge and with whom I worked shoulder-to-shoulder designing, preparing and executing the electrochemical field experiment described in this dissertation.

My gratitude also goes to CONACYT the Mexican science and technology office for partially sponsoring my studies at Imperial College London.

I want to express my especial gratitude to my wonderful family, which always supported me and were my cornerstone not only during this project, but for the entire year in the course of my Master Degree studies.

Last but not least, I want to express my deepest gratitude to my wife, Susana Velazquez who has being with me side-to-side on the distance sharing tears and laughs throughout the year.

Contents

List of Figures

List of Tables

Imperial College London

Field Measurements of spontaneous potential (SP) for smart well monitoring and control. A field test in the UK chalk aquifer.

Armando Esquivel García

Imperial College Supervisor: Prof. M.D. Jackson, Prof. A.P. Butler, J. Vinogradov, D.J. MacAllister.

Abstract

Spontaneous potential (SP) has been extensively used since the early days of oilfield exploration for identification of permeable zones and formation water salinity. However, recently SP has being finding a place in new proposed applications, e.g. monitor waterfront towards producing well during flooding operations and monitor seawater intrusion in fresh water aquifers in coastal areas. For oilfield reservoirs, the possibility of monitoring the waterfront towards the production well during flooding operations will help to implement a control system which will prevent or regulate the water breakthrough. This document presents the results of the field experiments for the electrokinetic (EK) and electrochemical (EC) components of SP in chalk aquifer in the Bottom Barn Abstraction (BBA) in Berkshire UK. The electrokinetic results were obtained during pumping conditions yielding a coupling coefficient of -97 ± 40 mV Mpa-1 which is consistent, in the error range, with the value of -60 ± 13 mV Mpa-1 obtained in laboratory tests. The electrochemical experiment consisted of the injection of brine with a concentration near a third of the salinity of the seawater. Four salt dumps were held in four consecutive days. A voltage response was measured for the first two salt dumps, later related to a redox potential response due to the metallic completion in the dump borehole in contact with the water top. Further dumps were done in plastic casing with no evidence of voltage response (i.e. EC response). The conductivity profiles may provide a link with the EC experiment results, suggesting that the concentration might have settled in the matrix or diffuse through the fracture network, thus the brine was rapidly dispersed and did not reach the monitoring wells. The result of the EK experiment confirms the possibility of monitoring the groundwater flow in field conditions to control and prevent water encroachment from injected water during waterflooding operations in oilfields. Instead, NaCl mass poured into the borehole should be increased to produce a measurable EC signal. This will replicate real conditions when seawater encroaches onto an abstraction well or is injected into a borehole in a producing oilfield as part of waterflooding operations.

Introduction

Spontaneous potential (SP) measurements have been used since the early days of electrical oilfield exploration prior to production to identify permeable zones, which potentially leads to the detection of oil bearing rocks (Deussen & Leonardon, 1935). The Schlumberger brothers were the first who commercially offered this service in 1931, together with resistivity recordings (Johnson, 1962). Initially, they explained the SP occurrence by effect of the streaming potential (i.e. electrokinetic or EK potential) which has its origin in the pressure gradients in fluids (Mounce and Rust, 1944). It was later when they concluded that SP was a result of the combined effects of electrochemical (EC) and EK potentials, attributing to EC the major contribution to total SP. EC potential is caused by contrast in salinity between drilling and formation fluids (Wyllie, 1951). Later Tasaka *et al.* (1965) described the thermoelectric potential (TE) which is caused by difference in the temperature between the injected and the reservoir fluids (Revil, 1999).

When a gradient of the chemical composition, pressure or temperature generates a separation of electrical charges, SP acts in order to maintain electroneutrality (Marshall and Madden, 1959; Corwin and Hoover, 1979; Revil, 1999). In a water-wet reservoir rock, charge separation occurs when the water reacts with the mineral surface, leaving an excess of charges in the water adjacent to the mineral surface (Wyllie 1951). This charge layout is known as the electrical double layer (Hunter, 1981). The charges on the mineral surface (typically negative), which form the Stern layer, are hydraulically immobile. Thus, the counter ions are in excess in the diffuse layer. These charges are mobile, and will move with the fluid. If the water is subjected to a pressure gradient that causes the fluid to flow along the mineral surface, some of the charges will move with the flow triggering a streaming current. In order to equilibrate this streaming current, a conduction current is then raised. To keep this conduction current a voltage is generated. This potential is called the streaming potential or electrokinetic (EK) potential. Jackson *et al.* (2012b) shows this process in Fig. 1a**.**

In the case of EC the composition variations leads to concentration gradients which cause ionic species migration (Fig.1b). In some cases mobility of the ions is different, e.g. in NaCl the sodium ions move 30% slower than those of chloride at 25^{o}C (Braun & Weingartner, 1985). The electroneutrality is achieved by EC potential which counteracts the charge separation (Revil, 1999). The EC potential can be originated if the solid surfaces are charged or not. If it is charged, an electrical double layer at the mineral/water interface explains that some of the ions in the brine are excluded from the pore

space, so an excess of positive charges migrates down the concentration gradient (Ortiz *et al*, 1973). This gives rise to an exclusion potential. In the other case, being the solid surface uncharged the EC potential will be only attributable to diffusion potential or liquid junction due to the difference in ionic mobility.

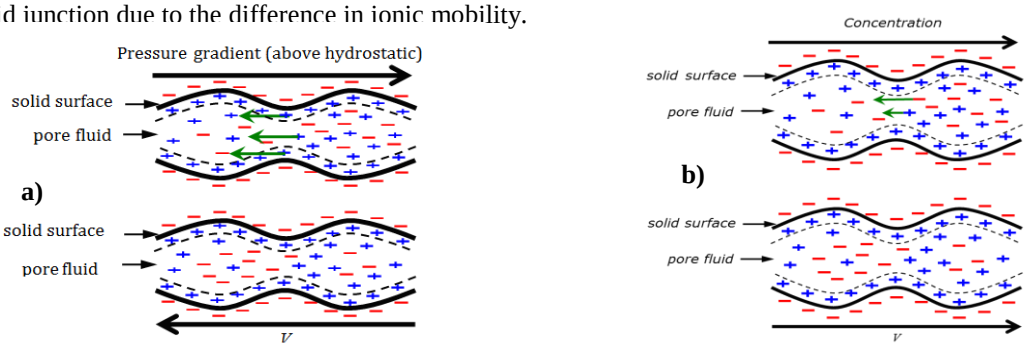

Fig. 1 Schematic of the separation of charges at the mineral/water interface and the origin of **(a)** EK and **(b)** EC potential. (Jackson *et al*, 2012b)

The TE potential is generated by temperature gradients derived from the variations in fluid temperature. The differing mobility of ions caused by this temperature gradient and exclusion of co-charge from the pore-space produces a separation in the charges. The electroneutrality then is maintained by the thermoelectric potential which counteracts this charges separation (Tasaka *et al.*1965; Revil, 1999).

In recent years the use of SP for exploration purposes has being slowly displaced in the oilfield exploration and characterisation by new technologies like resistivity, the use of radioactive tools and borehole imaging. Despite this, SP has being finding a place in new applications, e.g. corrosion detection in producing oil wells (Kendall, 1961) and reservoir fluid monitoring derived from electrokinetic (EK) potential measurement (Darnet *et al*. 2004). Saunders *et al.* (2008) suggests the use of SP measurements to detect water encroachment towards intelligent wells with permanently installed electrodes. Numerical reservoir models proposed by Saunders *et al.* (2008) and Jackson *et al.* (2012b) suggests that the produced SP signals in a hydrocarbon reservoir during waterflooding operations can be up to hundreds of millivolts, allowing to image groundwater movement in instrumented wells from tens to hundreds meters before water breakthrough. This simulated SP is dominated by EC and EK potentials before water enters the borehole (Jackson *et al.* 2012b).

During hydrocarbon production gradients in pressure, chemical composition and temperature will be present in the reservoir due to production techniques such as water (waterflooding) or steam (steamflooding) injection, triggering the occurrence of SP signals (Jackson *et al*, 2012b). These signals can be monitored installing electrodes in boreholes or in Earth's surface (Hunt & Worthington, 2000) making it, in the latter case, a non-intrusive technique. Chen *et al* (2006) demonstrated that SP measurements can be acquired using permanently installed downhole electrodes in open-hole wells and cased–hole wells with insulated steel casing. Jackson *et al.* (2012a) successfully measured SP signals generated by a pumping experiment using an array of borehole and surface electrodes in the Seaford Chalk formation in Berkshire. Part of the work here reported is based on the success of this initial observation.

This work refers exclusively to the measurements of EC and EK potentials for the water front monitoring towards boreholes for control purposes. The thermoelectric potential is discarded since according to reservoir model simulations done previously (Gulamali *et al*, 2011; Jackson *et al.* 2012b) TE potential can be very high in the temperature front associated to the waterflooding operation. However, the temperature front will lag behind the water front due to slow heat diffusion into reservoir rock. Thus a significant SP signal, enough to monitor the underground moving fluids, will be measured just after water reaches the production well. The shallow chalk aquifer described in this work was used because it was accessible and is geophysically characterised (e.g. Mathias *et al.* 2007 and Butler *et al.* 2009). The use of an oilfield for experimental purposes is much more challenging logistically and in availability. Yet, the results obtained of these experiments suggests that SP measurements can be properly acquired in instrumented boreholes of different oilfield reservoirs, although cannot be taken as analogue to other reservoir types. This is because the surfaces charges are different for distinct minerals (Saunders *et al.* 2009).

Another benefit of this experiment is related to studies on seawater intrusion in coastal aquifers. According to Abd-Elhamid *et al.* (2008) seawater intrusion into coastal aquifers is considered one of the most serious impacts of sea level rise. This intrusion can lead fresh water aquifers to become saline, affecting the population which depends on the water abstracted from these aquifers. The measurement of EC produced by the salinity contrast between fresh water in aquifers and the seawater can help to monitor the saline water front and prevent the increase of salinity in abstraction boreholes.

The aim of this work is to produce EK and EC potentials by means of pumping and brine injection field experiments in a chalk aquifer in Berkshire UK. Also to estimate the EK coupling coefficient of the pumping experiment. The coupling coefficient is a relationship of changes in voltage and fluid pressure when total current density is zero (e.g. Sill, 1983)

$$C_{EK} = \left.\frac{\partial V}{\partial P}\right|_{j=0}$$

The objectives of these experiments are to compare the resulting field coupling coefficient of EK potential with the

laboratory results (Jackson *et al.*, 2012b) and verify the possibility of occurrence of EC potential caused by a change in salinity. Similarly, these experiments will investigate if the SP signal monitoring can be used to characterise aquifer properties and groundwater flow in the chalk aquifer, as well as a proof of concept for long term reservoir monitoring during waterflooding or steam injection.

The experiment site: Bottom Barn Abstraction Berkshire, UK

The place for the experiments is situated in the Berkshire Chalk aquifer in Berkshire UK (Fig. 2 and Butler *et al*, 2009), where six 100 m deep vertical boreholes (PL10A to PL10F) were drilled around an abstraction well managed by the UK Environmental Agency as part of the UK Natural Environment Research Council thematic programme on lowland catchment research (LOCAR; Wheater and Peach, 2004; Fig. 3). Two of them (PL10B and PL10E; see table 1) are for observation purposes. PL10A was completed with metallic surface casing until *c.* 90 m Above Ordnance Datum (AOD); this is 0.5 m lower than the measured water table (Table 1). PL10B and PL10E were completed with plastic casing to surface. The other three wells (PL10C, PL10D and PL10F) were not used during this field experiments since they were equipped with piezometers by the Environmental Agency. The site is located on the side of a dry valley on the Chalk outcrop (fig.2).

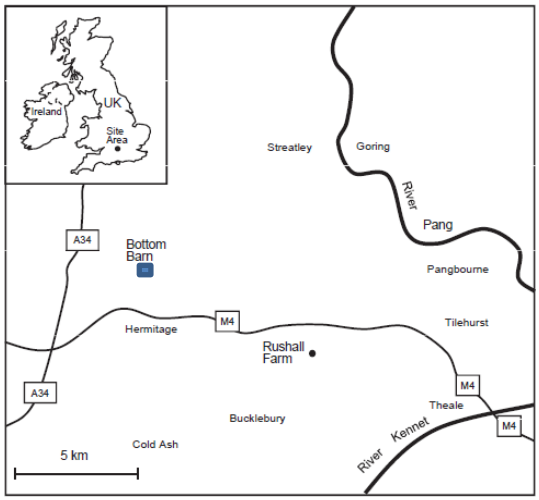

Fig. 2 The Bottom Barn Abstraction location. (Jackson *et al.* (2012a).

Table 1. *Location coordinates and elevation of boreholes at the field site (Butler et al, 2009)*

Borehole	Easting	Northing	Elevation (m AOD)	Water Table (m AOD)
PL10A	451304.8	175029.6	107.79	90.45
PL10B	451320.4	175063.1	110.51	90.2
PL10E	451343.7	175044.1	107.47	90.09
BBA	451330.0	175010.0	105.75	*

* It was not possible to measure the depth to the water table from surface in the BBA since access to a measure point was not granted.

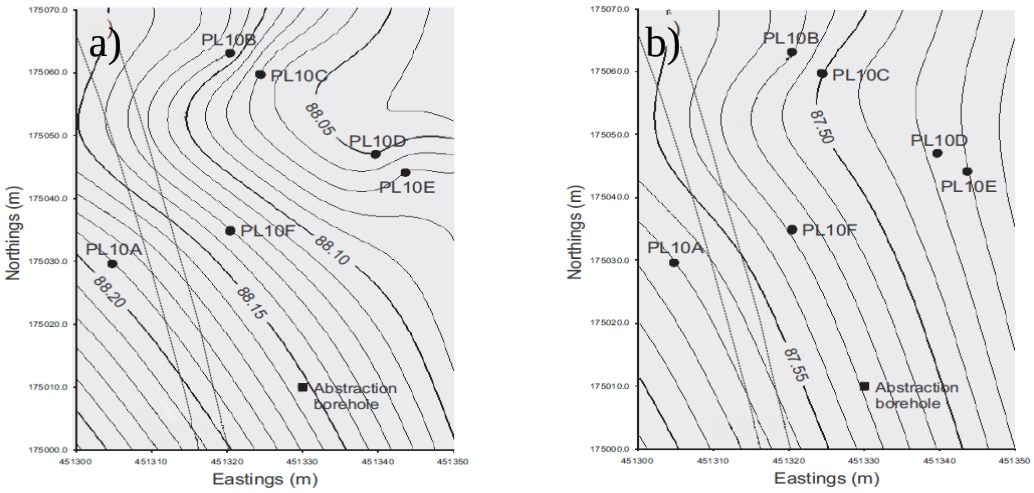

Fig. 3 Simplified map showing locations of boreholes in the BBA. Plot (a) and (b) show the groundwater level contours at different times taken before previous field experiments. The measurements are referenced to mAOD (meters Above Ordnance Datum). Dashed lines symbolises a rural road. The black circles represent borehole locations and the filled square refers to the abstraction borehole. (Jackson *et al* 2012a)

The Berkshire Chalk lithostratigraphy was revised in 1999 by the British Geological Survey (Butler *et al*, 2009), comprising a new classification adding the Chalk Rock which is a 3m bed of phosphatized and glauconized chalk-pebble intraclasts near the base of the Lewes Nodular Chalk (former Upper Chalk). This bed can be identified by a peak in the gamma

ray (GR) counts (Schurch and Buckley, 2002; Fig. 4), on the top of this bed is all Seaford Chalk. The logs available in Fig. 4 were acquired from borehole PL10A attending several efforts to characterise the chalk formation in this borehole together with PL10B; the information was taken from flow and geophysical logging (GR, televiewer, etc.), dilution test and packer test (Williams *et al*, 2006; Mathias *et al*, 2007; Butler *et al*, 2009). The EK and EC experiments reported heres were conducted inside the Seaford Chalk boundaries.

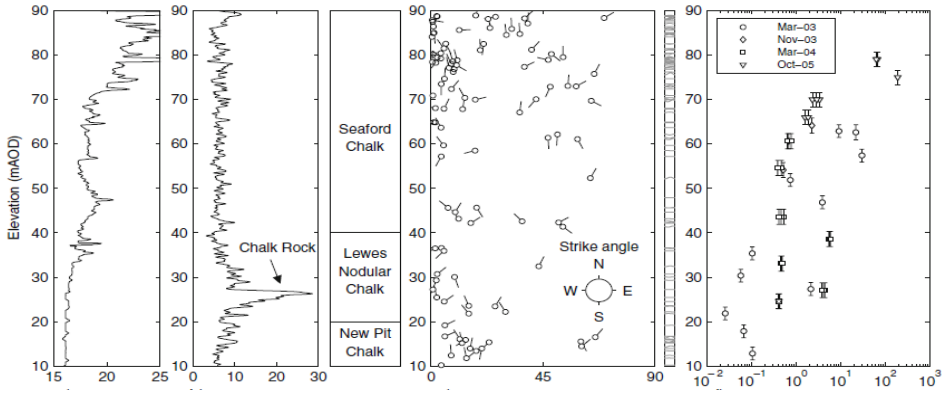

a) Caliper (cm) b) GR log (GAPI) c) Fracture dip angle (degrees) d) Hydraulic conductivity (m/day)

Fig. 4 Borehole PL10A geophysical properties. a) Caliper logging showing borehole variations with depth. b) GR log. Note the Chalk Rock bed *c.* 24 m AOD. c) Tadpole plot derived from televiewer, providing fracture dip and strike. d) Hydraulic conductivity profile derived from constant head double-packer permeater test (Butler *et al.* 2009).

The Chalk aquifer in BBA is a dual-porosity aquifer with a microporous matrix intersected by fractures (Price 1987; Price *et al.* 1993). The main path for the flow is provided by the fractured matrix (Fig. 4 c & d), since the absolute matrix permeability to water lies in the order of 2 mD (Price 1987; MacDonald *et al*, 2001; Table 2).

Previous pumping experiments at constant rate inducing drawdown in the abstraction well and pressure build-up when pumping was stopped, delivered estimations of effective transmissivities using the Jacob's method on the late time data (Meier *et al*. 1998), stating that despite the scale of the test compared with the size of the aquifer, the formation is likely to be homogeneous and isotropic, with negligible wellbore storage. The monitored flow obeys Darcy's law and the effects of elastic storage and delayed yield can be ignored (Butler *et al*, 2009). From the effective transmissivities for this field (Butler *et al.* 2009) an estimation of effective permeability can be done according to Oosterbaan *et al.* (1994). The effective permeability estimated, assuming an aquifer thickness of 90 m ranges from 33 to 58 Darcys. Another approximation taking an average of the hydraulic conductivity data from Butler *et al.* 2009 (Fig. 4) estimates a value of 26 Darcys (see appendix E).

From the flow meter and dilution tests, it was found that a substantial upflow from the bottom of the PL10A well was present. Several inflow and outflow depths were also identified for PL10A and PL10B (Figure 5; Mathias *et al.* 2007, Butler *et al.* 2009). This will prove to be important in our experiments, since these inflow and outflow profiles are associated to high permeability fractures, thus suggesting a possible communication path between boreholes.

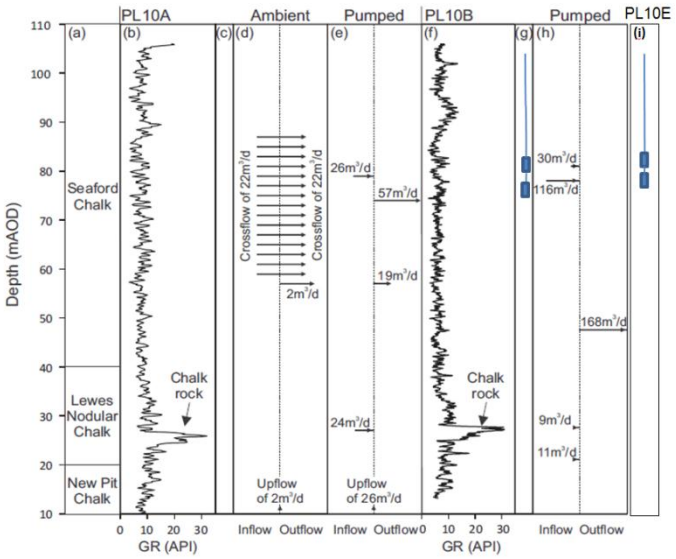

Fig. 5 PL10A, PL10B and PL10E general information. All geophysical data was previously acquired (Mathias et al, 2007; Butler et al, 2009; Jackson et al, 2012a). **(a)** Lithology column. **(b)** Natural gamma ray log. **(d)** Crossflow at ambient conditions. **(e)** Crossflow at pumped conditions. **(f)** Natural gamma ray. Note the spike correlation of the Chalk Rock at the same depth for both wells. **(g)** Location of borehole electrodes (BE) in PL10B for EC experiment. **(h)** Crossflow interpreted at pumped conditions. Ambient data for PL10B is not available. **(i)** Borehole electrodes location in PL10E for EC experiment.

Table 2 *Properties of Seaford Chalk sample used in laboratory experiments (Jackson et al, 2012a).*

Property	*Value*
Absolute permeability to water (*K*) mD.	2.28
Porosity (ϕ), %	35
Electrical conductivity when saturated with groundwater (σ). S m^{-1}	0.026
Formation factor (FF) (dimensionless)	6.12

Field measurement of electrokinetic potential

Methodology

The experiment was divided in two parts, the pumping and the ambient conditions. The pumping stage was held from February 28th, 2011 to March 8th, 2011. Ambient conditions were measured from March 8th, 2011 *c.* 12:00 hrs. to March 15th, 2011. The measurement strategy involved a surface electrode array comprising monitoring electrodes. Each electrode is a non-polarizing Ag/AgCl electrode and measures 205 mm length × 30 mm diameter. Every electrode consists of an Ag wire skeleton with a porous silver matrix formed around. This silver matrix is coated with AgCl. This arrangement is embedded in a 0.05 M KCl gel for borehole electrodes (BE) and 0.5 M KCl for surface electrodes (SE). In both electrode types, a low-permeability porous disc provides the path to electrically connect the gel to the outer environment (www.silvion.co.uk).

The surface electrode array was formed by fourteen non-polarizing SE located in a crossed pattern, with a separation of four meters between them. SE electrodes were placed from the abstraction borehole to PL10B and from PL10E in direction to PL10A (Fig. 6). Two more borehole electrodes (BE1 and BE2) were installed inside borehole PL10B. One more SE was installed far away (*c.* 90 m) from the experiment site to serve as a reference electrode. This will prevent the electrode from being affected by the changes in voltage caused by the electrokinetic potential in response to the pressure gradient generated by the pump at the abstraction borehole. This will allow comparing the reference electrode with the measurements from the surface and borehole electrodes in the experiment site and identifying any possible response related to the experiment performed. To isolate the electrodes from temperature change and external electrical noise, every electrode was installed in a pit in the soil at *c.* 0.2 m deep. (See details in fig. 7); this arrangement improves the electrical connectivity between the soil and the electrode and provides electrical stability against any ambient interference (Kostic *et al*, 1999; Fig. 7).

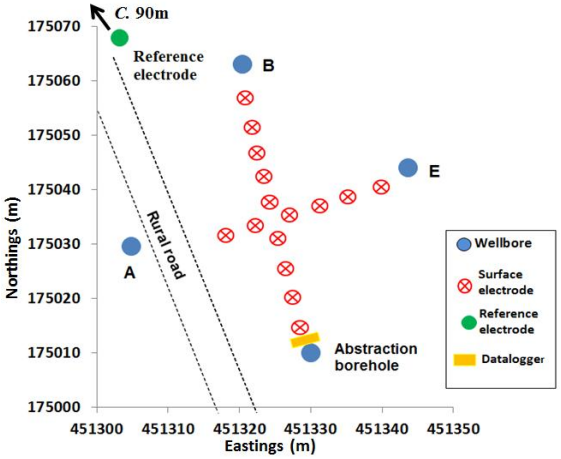

Fig. 6 Location of the surface electrode array in the BBA experiment site for EK potential experiment. Blue circles denote the borehole locations. The crossed-circles symbolise the surface electrode location.

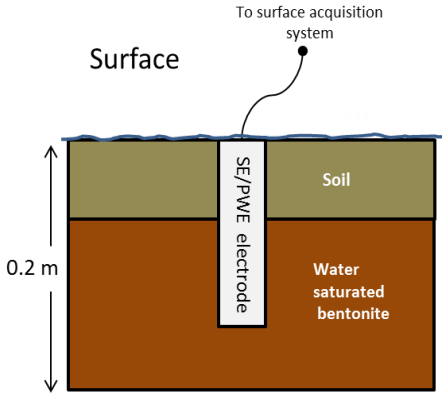

Fig. 7 Borehole/surface electrodes installation procedure.

In the abstraction borehole, water was pumped with an average of 54 × 10^3 bbl/d of water for eight consecutive days and the voltage monitored. Then, pump was switched off and monitoring continued for ambient conditions for the following seven days, until March 15th *c.* 10:00 hrs. In figure 8 the pressure drawdown-buildup and the pumping rate are correlated. A pre-pumping stage prior the experiment caused initial pressure to be smaller than the final pressure.

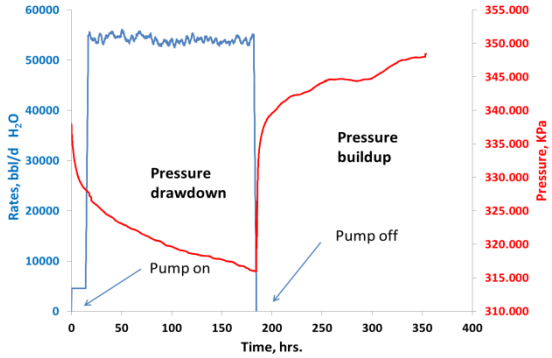

Fig. 8 Pressure response in PL10B to changes in rates in BA through the extended pumping period.

A temperature probe was installed to record the temperature changes during the complete test. The probe was installed next to the datalogger. The datalogger location can be seen in Fig. 6. All electrodes and the temperature probe were connected to DL2 datalogger (internal impedance 100 MΩ, resolution 64 µV, accuracy 0.07%) from Delta T devices.

Electrokinetic Experiment Results and Discussion

The data collected from the surface electrodes did not show any conclusive response (i.e. measurements above 200µV or background noise) to ambient or pumping conditions (fig. 9a & 9b). Borehole installed electrodes provided a clearer response to pressure changes (fig. 10).

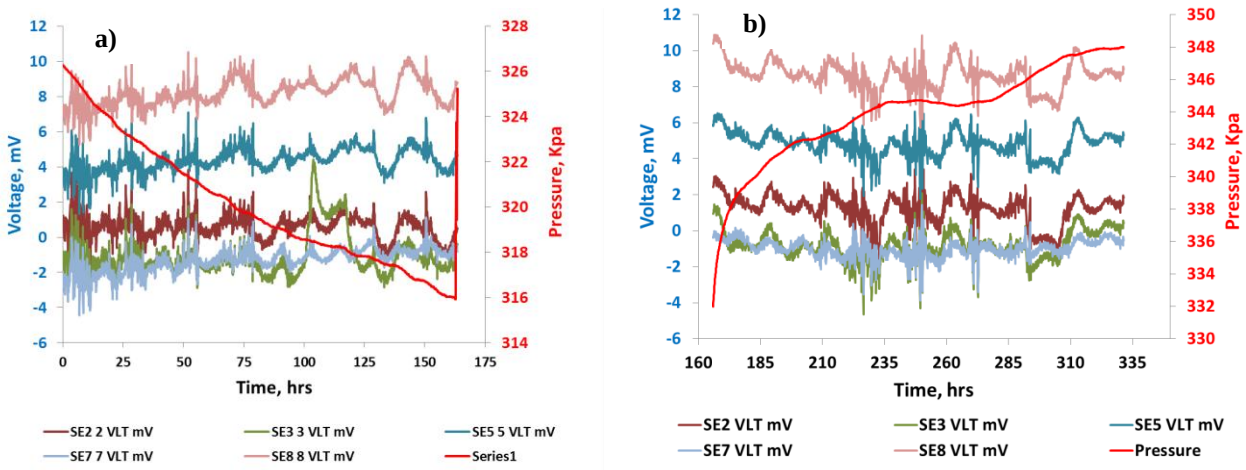

Fig. 9 Surface electrode response to **(a)** pressure drawdown, i.e. pump is turned on and **(b)** Pressure buildup, i.e. pump is turned off

The analysis for borehole electrodes showed a clear response to pressure change for BE1 and BE2, both installed in borehole PL10B. Despite BE1 is showing the same tendency after 75 hrs. early data shows a difference between BE1 and BE2 reflecting a stabilisation phase for BE1(Fig. 10 in green). However, the study was devoted to analyse the data coming from BE2 borehole electrode since it showed a consistent response since the beginning of the experiment (e.g. no stabilisation time).

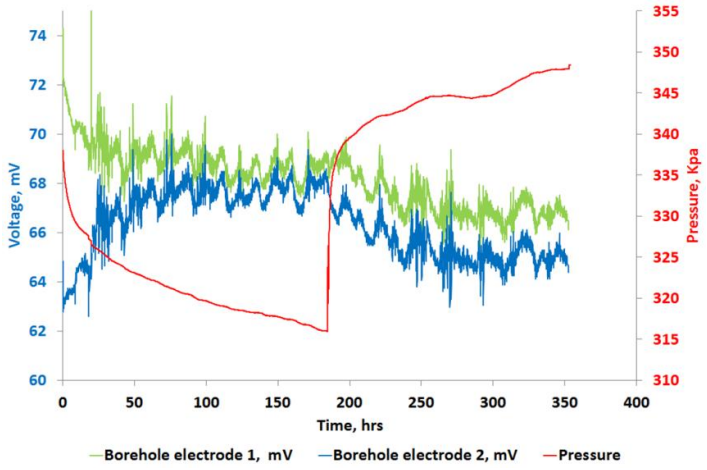

Fig. 10 Borehole electrodes response to pressure gradient. Note voltage response of BE2 (blue) to pressure gradient in comparison to BE1 (green) which shows a stabilisation phase.

The data acquired from the electrodes is clearly influenced by the temperature cycles (e.g. BE2; Fig. 11a). The electrodes were particularly sensitive to this effect due to the shallow depth at which they were placed. In figure 11b, the temperature effect on the voltage response is clear and can be seen that, at least in a limited range of time, is affecting the data collected. However, in other section of the same dataset a proper correlation between the voltage and the temperature cannot be established. This is attributed to the separated location of the temperature probe (next to the datalogger) regarding the borehole electrodes, thus the voltage variations caused by the temperature changes in the electrode could not be correlated with the temperature variations of the temperature probe.

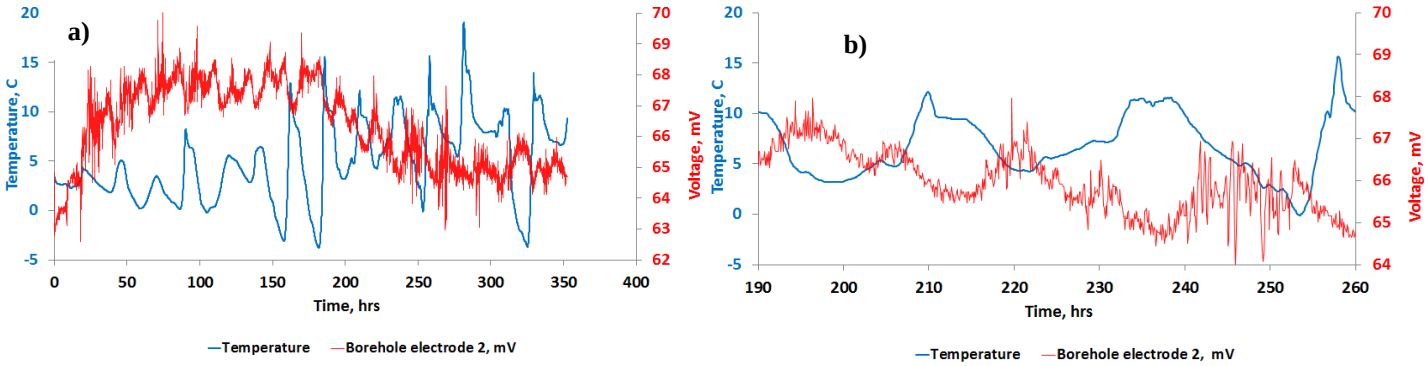

Fig. 11 Temperature effect on BE2 electrode response. **a)** Plot showing the entire range of data. **b)** A clear effect of temperature in the voltage measurement in a section of the dataset. However, this effect was not consistent on the entire range of data.

To minimise the effect of temperature on voltage, several correlations were tried. However, as voltage and temperature were measured at different location no simple correlation was obtained. Due to this we use moving averages with 25 data points to minimise high frequency noise (Fig. 12a). Then we used the *butt* and *filter* utilities in MATLAB® to apply a Butterworth filter (see Appendix C) to smooth out the temperature effect (fig. 12b). Despite the temperature was not entirely de-trended, in the resulting data the dominant voltage response is due to the change in pressure (Fig. 12b).

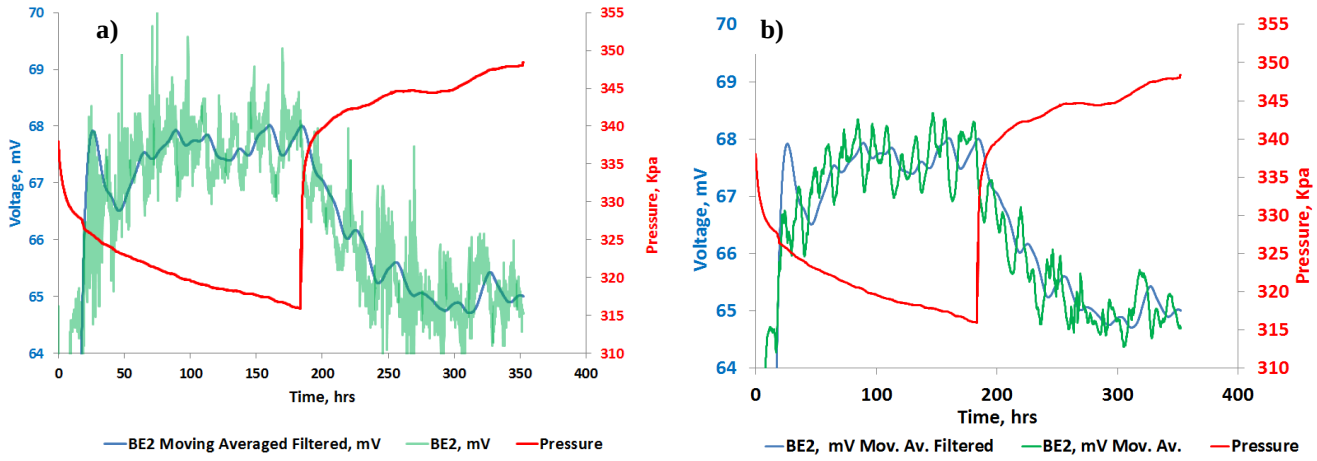

Fig. 12 BE2 borehole electrode response to pressure gradient. **(a)** Moving averaged voltage (blue) and raw voltage data (green). **(b)** Plot showing the resultant filtered signal (blue).

However, the slow decay in the voltage measurement during the pressure build up (i.e. when pump was set off) still interferes with the coefficient determination, which denotes a contrast with laboratory experiments (Jackson *et al*, 2012a). Laminar flow assumes that the flow near a production well is dominated by viscous forces, neglecting gravity and capillary pressures (e.g. Dake, 1978; Shook *et al*, 1992), thus a sudden change in pressure will also cause a change in the flow in (or close to) the same time frame. However, in the case of the field experiment the inertial forces induced by the large flow rates (*c*. 54×10^3 bbl/d) through approximately eight days cannot be neglected, thus the slow decay could be due to water movement in the matrix driven by this inertial forces even with no apparent pressure gradients. The effect in the delay on voltage response and the slow decay of the pressure gradient in the aquifer was observed as well in further streaming potential experiments; e.g. Chen *et al* (2006) shows a similar slow voltage response to pressure changes in a vertical injection well.

The coupling coefficient was obtained from the plot of voltage and pressure selecting two representative sections of stabilised pressure and voltage from the entire data set. These sections were chosen from the most stable zones (i.e. not affected by the slow voltage response) as can be seen in figure 13. Figure 14 shows the plot of pressure versus voltage and the coupling coefficient value of -97 ± 40 mV MPa^{-1} estimated by linear regression. The error bars in the plot displayed in figure 14 represents the variation in the voltage measured in the borehole. With this variation a higher (blue) and lower (red) case of the EK coupling coefficient can be estimated and provide an error range (fig.14).

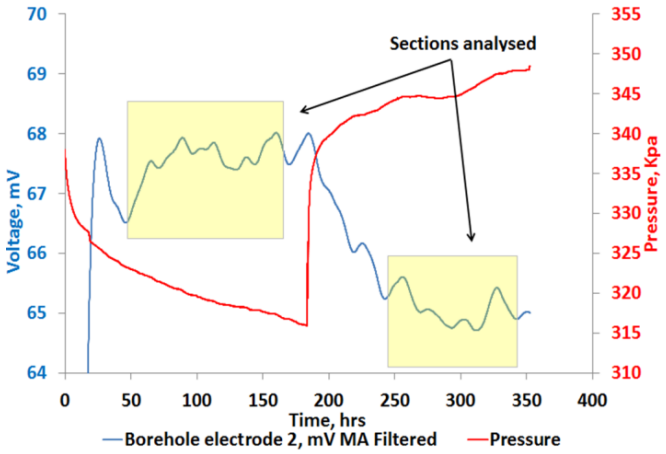

Fig. 13 BE2 voltage sections used for coupling coefficient determination. Sudden pressure build up and slow voltage response.

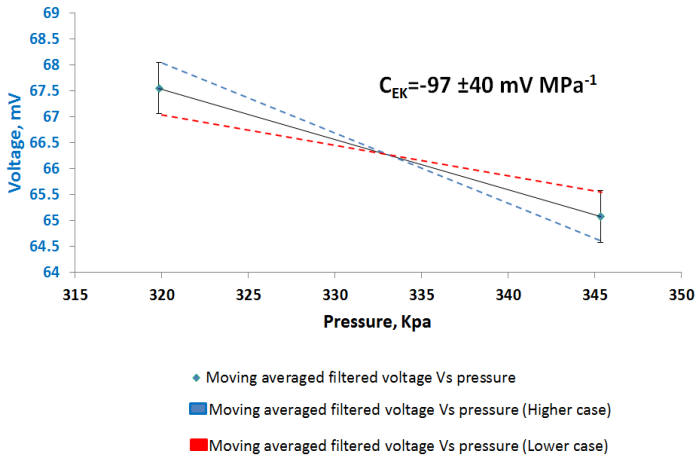

Fig. 14 EK coupling coefficient and error determination.

This streaming coupling coefficient measured in the field (-96 ± 40mV MPa^{-1}) is same, within experimental error, to the laboratory results of -60 ± 13mV MPa^{-1} (Jackson *et al*, 2012a). Thus we can say that the field experiment confirms the results obtained in the laboratory.

Field measurement of electrochemical potential

Methodology

The aim of this experiment was to simulate the salinity gradient caused by a waterfront of different salinity injected into a fresh water aquifer in waterflooding operations in order to yield and measure an EC potential. To generate this potential, injection of NaCl brine in borehole PL10A was proposed. The wellbores involved in this experiment were PL10A, PL10B and PL10E. According to the measurements of water tables previously done (Jackson *et al*, 2012a) and recent measurements; fig. 3; fig. 1), water table was higher in PL10A, thus suggesting a hydraulic gradient driving the flow from PL10A to PL10B and PL10E. Due to this, PL10A was chosen as the brine injection well. PL10B and PL10E were assigned as monitoring wells.

To improve the possibility of capturing EC signals according to the flow patterns (fig. 5), a different installation of surface electrodes (SE) was proposed compared to the electrokinetic experiment described in this document. To achieve this, an array consisting of three soil electrodes was placed in a linear pattern from the monitoring wells (PL10B & PL10E) towards the injection well (PL10A). To install the surface electrodes, a *c.* 0.5 m deep hole was dug for every surface electrode to isolate the electrodes from temperature drift effect and any external electrical disturbance. The surface arrangement is shown on fig. 15. A plastic bucket was used in the installation to improve the stability of the electrode measurements (Perrier *et al*, 2005). The buckets were filled with water-saturated bentonite to improve the electrical conductivity (Kostic *et al*, 1999). Details on installation can be seen in figure 16. An extra soil electrode was installed together with a temperature probe to serve as reference electrode. It was located *c.* 80 m from the surface acquisition system (fig. 15) at the same location as the reference electrode in the electrokinetic experiment. The temperature probe was used to register any temperature change that could be later related to any voltage drift in the electrodes caused by temperature.

Two downhole electrode arrays were comprised of two borehole electrodes (BE) with three meters separation distance. This design was conceived to capture the main cross flow according to the geophysical log for each well (i.e. crossflow in Fig. 5), assuming the same conditions of PL10A for PL10E. Figure 5 denotes the location of the borehole electrodes in PL10B (BE1 & BE2) and PL10E (BE3 & BE5). One more array involving a borehole electrode and conductivity probe was set up and used as a travelling tool for vertical borehole profiling. This tool provided conductivity, pressure, temperature, and voltage and was used to do variable depth borehole profiling (i.e. run in and out of borehole while measuring the mentioned physical properties). This tool is termed "Travelling electrode". The surface and borehole electrodes were identical to the used for the electrokinetic field experiment previously explained.

Another conductivity probe was assigned to borehole PL10A for depth measurements and conductivity profiling. The conductivity profile can help to identify the flow patterns inside the borehole (Butler *et al.* 2009). In this experiment, one of the conductivity probes was used to trace the salt dump behavior in the borehole due to the high contrast in salinity with the fresh water in the aquifer. The conductivity probes (Aqua-troll 200) were acquired from In-Situ Inc.

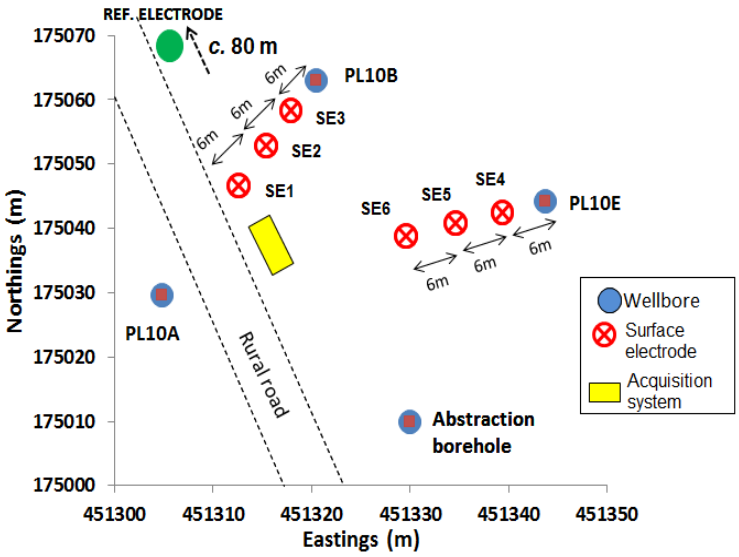

Fig. 15 Map location for boreholes and surface electrodes.

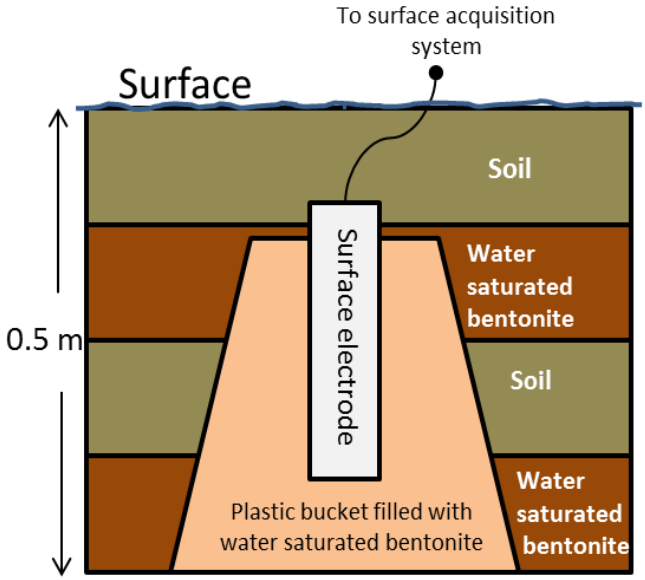

Fig. 16 Surface electrode installation

method. The dashed lines denote a rural road.

Except for the conductivity probe assigned to manual conductivity profiling of the injection well, which was directly connected to a portable computer, all the electrodes were connected to a surface data acquisition system CR3000 from Campbell Scientific.

The background measurement (i.e. voltage measurements in ambient conditions) was initiated the 13/07/13 and was stopped in 16/07/13 *c.* 11:00 hrs. to proceed with the salt dump. A salt dump was performed on four consecutive days (I-IV; table 3). Permission from the Environmental Agency was required and granted to run this experiment. The concentrations varied in each dump according to table 3. The maximum concentration in the borehole was limited to one third of the seawater concentration (i.e. *c.* 0.17 M). Borehole PL10E was used as a monitoring well for the entire experiment. PL10A was initially used for salt dump, however due to the occurrence of redox potential associated to the metallic casing in the same borehole, the last two salt dumps were conducted in PL10B.

The dump number I (see table 3 for details) was held on September 16th, 2013 at 15:13 hrs. in PL10A. The concentration of the brine injected was 210 gr/L (210,000 ppm) which lead to a borehole concentration of 9.93 gr/L or 0.17M, (see Appendix B for salinity calculations). Vertical profiling was conducted with the travelling electrode tool in PL10E and PL10B, and PL10A was profiled for conductivity after the dump. Conductivity profiles were also carried out in the three boreholes for reference purposes prior to the dump. The outcomes are discussed in the results section.

Table 3 *Schedule of salt dumps and boreholes. Molarity included.*

Dump number	Date	Borehole	Salt mass	Mol (gr/L)
I	16/07/13 15:13 hrs	PL10A	31.5 Kg dissolved in 150 L tap water	9.93
II	17/07/13 14:40 hrs	PL10A	18.5 Kg NaCl solid state	6.1
III	18/07/13 17:41 hrs	PL10B	19.5 Kg commercial NaCl solid state.	6.5
IV	19/07/13 12:42 hrs	PL10B	25 Kg NaCl solid state	8.3

The salt dump number II (table 3), was performed on September 17th, 2013 at 14:40 hrs in PL10A. Borehole arrays for PL10B and PL10E were modified for depth in order to expand the range of crossflow monitoring. PL10B electrodes (BE1 & BE2) depths were *c.* 89 m AOD and *c.* 78 m AOD respectively and PL10E electrodes (BE3 & BE5) were *c.*87 m AOD and *c.* 76 m AOD. The same profiling routines as per the first dump were conducted in each borehole.

The salt dump number III was done on September 18th, 2013 at 17:41hrs in PL10B. The permanent installed electrodes in PL10B were changed to PL10A and the conductivity profiling was held in PL10B.

Dump number IV was performed in September 19th, 2013 at 12:42 hrs. Salt dump was performed in PL10B, subsequent conductivity profiling was performed in this well. PL10A remained as per salt dump III.

Electrochemical experiments results and discussion:

The data collected from the surface electrodes in salt dumps I and II was associated with redox potential since the necessary

conditions, as the salinity gradient and the ore body (metallic casing in PL10A) were present (Sinnott, 2005; Jouniaux *et al*, 2009). This was later confirmed by salt dumps III and IV, where no voltage signal was measured due to the plastic casing in PL10B. In redox potential electrons are generated by oxidising and reducing reactions occurring at the bottom and the top of the casing, then transported through the metallic casing which acts as a conductive medium (Jouniaux *et al*, 2009). The borehole PL10A is completed to the surface, thus electrons generated are conducted to the surface and propagated through the soil. Figures 17 and 18 show the response of surface electrodes in the two consecutive days for redox potential response; however borehole electrodes didn't show any convincing response. According to the attenuation of the voltage in function of the distance from the source (PL10A) detected by the surface electrodes, the voltage amplitude was attenuated before it reached borehole electrodes in PL10B and PL10E. The figures 19a and 19b show the voltage amplitude attenuation with the distance from the source (PL10A) to the surface electrodes. The average rate of signal decrease was estimated in 0.06 mV/m. Over a distance of 18 m (distance from SE1 to borehole PL10B and SE6 to PL10E see fig. 15) the total attenuation is near 1 mV. The maximum amplitude at SE1 was of 0.96 mV thus no voltage could be measured by the borehole electrodes.

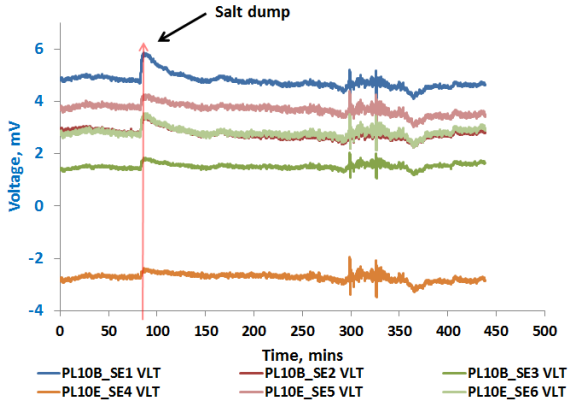

Fig. 17 SE response for first salt dump on July 16th 2013 at 15:13 hrs.

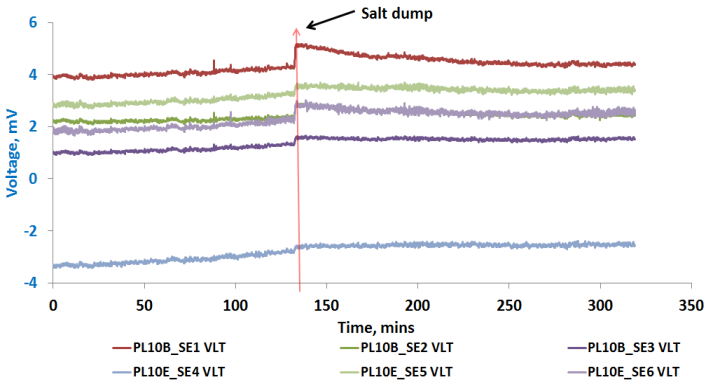

Fig. 18 SE response to second salt dump on July 17th 2013 at 14:40 hrs.

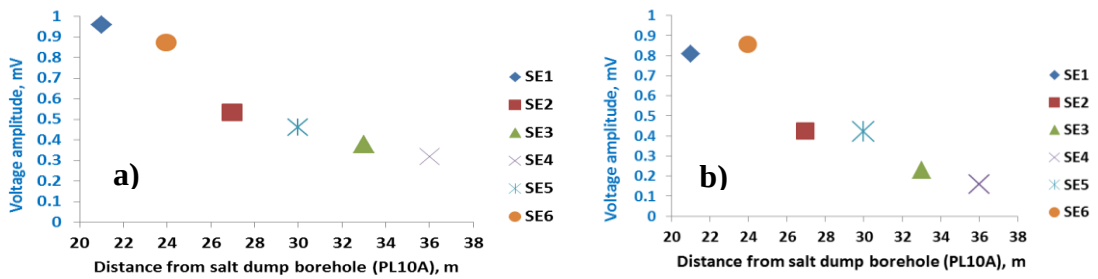

Fig. 19 Amplitude attenuation plots in PL10B. Plot **(a)** corresponds to 16/07/13 salt dump and plot **(b)** corresponding to 17/07/13 salt dump.

The difference in the redox voltage amplitude is directly related to the change in NaCl mass injected in the borehole, figure 20 shows the relationship between the mass poured in borehole PL10A and the voltage amplitude response measured by the surface electrodes.

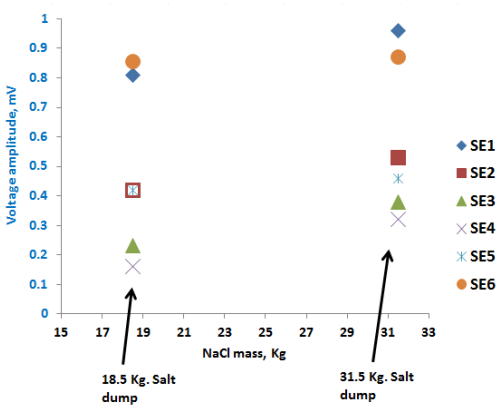

Fig. 20 Plot of voltage amplitude response to sodium-chloride mass poured in the wellbore.

The conductivity profiles in PL10A for both days showed a similar pattern. An evidence of crossflow in the conductivity logs from PL10A borehole can be related to the fracture set identified by Butler *et al* (2009; fig. 4). In these profiles (fig. 21a and 21b) it can be clearly observed that the major part of the salt concentration was diluted in the top ten meters after approximately two hours. The scales of concentration in the plots differ due to the different masses of salt dropped in the wells (see table 3); data is presented in specific conductivity which can be converted into molarity (see appendix D). The resultant profiles suggest the possibility that the fracture density at the top of the well (*c.* 80-90 m AOD) can be related with the fracture density reported by Butler *et al* (2009; fig. 4). The decrease in salt concentration when is in contact with fresh water in the aquifer, the fracture density at the top of the water table, the upflow in the borehole (Butler *et al*. 2009) and the crossflow in the formation (fig. 5) prevents the brine slug from moving downwards and being almost totally diffused in the first ten meters (fig. 21a and 21b).

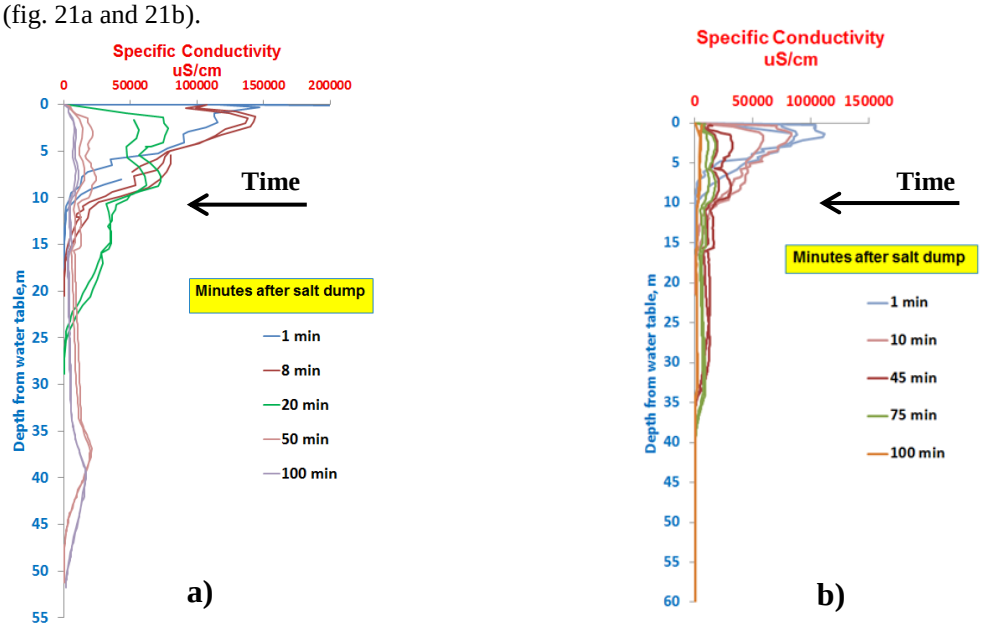

Fig. 21 Conductivity profiles for PL10A at **(a)** 16–07--13 and **(b)** 17-07-13. Depth is referenced to water table (i.e. 0 m is water table top). This well was used as injection well for two consecutive days.

The data acquired from the travelling array, which was used to profile PL10E and PL10B during salt dump I and II (see table 3), is shown in figure 22 (a-d). In the plots, it can be seen that conductivity measurements in PL10B does not show any change in the first 8-9 meters with respect to the conductivity profiles held before the salt dump (fig. 22b and 22d). From this is inferred that there is no interconnection with the fracture network. In contrast, a lower voltage response is perceived in PL10E in the first 2-4 meters, assuming that a possible connection through the fracture network could exist between PL10A and PL10E (fig. 22a and 22c). Also a difference in conductivity measurements can be seen between PL10B and PL10E. Despite the small value, as can be seen in the voltage plots, it can be an indicative of the fluid flow through the active fracture network for PL10E. It is important to note the voltage difference at the top 2-4 meters between PL10B and PL10E. This difference in measurements could be due to charges being move by water flowing through the fracture network in PL10E.

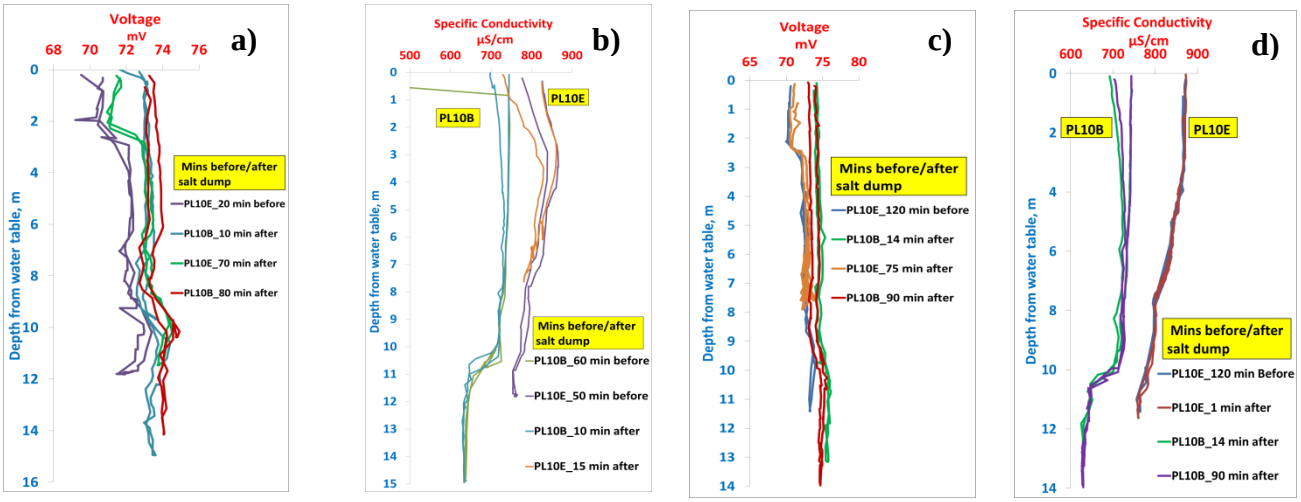

Fig. 22 Voltage and conductivity profiles acquired with travelling array for 16-07-13 **(a&b)** and 17-07-13 **(c&d)**. Note the separation between PL10B and PL10E. This is attributed to the effects of the flow in the active fracture network. Note: These shapes are typical for the totality of the measurements taken while profiling.

The salt dumps III and IV (*see* table 3) held in PL10B did not show a convincing voltage response (i.e. above background noise or 200µV) from surface or borehole electrodes (fig. 23a & 23b). Nevertheless, the conductivity profiles now performed in PL10B revealed the salt slug travelling to the bottom. The attenuation in conductivity signal in function of time, more noticeable in figure 24b, is possibly due to dilution. The pattern was repeated in dumps III and IV. This assumes that the inflow patterns obtained during pumping conditions (Fig. 5) are not present under ambient conditions, including the hypothesis that there is no upflow in PL10B due to the relatively fast displacement of the salt slug towards the bottom of the borehole (fig. 24a & 24b). Due to this, no evidence of crossflow in the borehole can be seen, thus inferring there is no interconnection between PL10A and PL10B through the fracture network in ambient conditions.

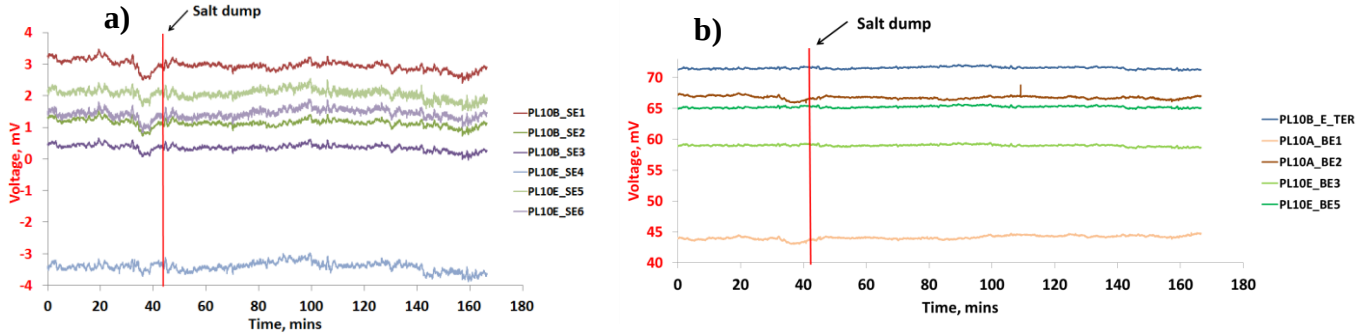

Fig. 23 Voltage response to salt dump in PL10B for **(a)** Surface electrodes (SE) and **(b)** Borehole electrodes (BE). Any possible response is in the background noise range, nearly 200 to 300 µV.

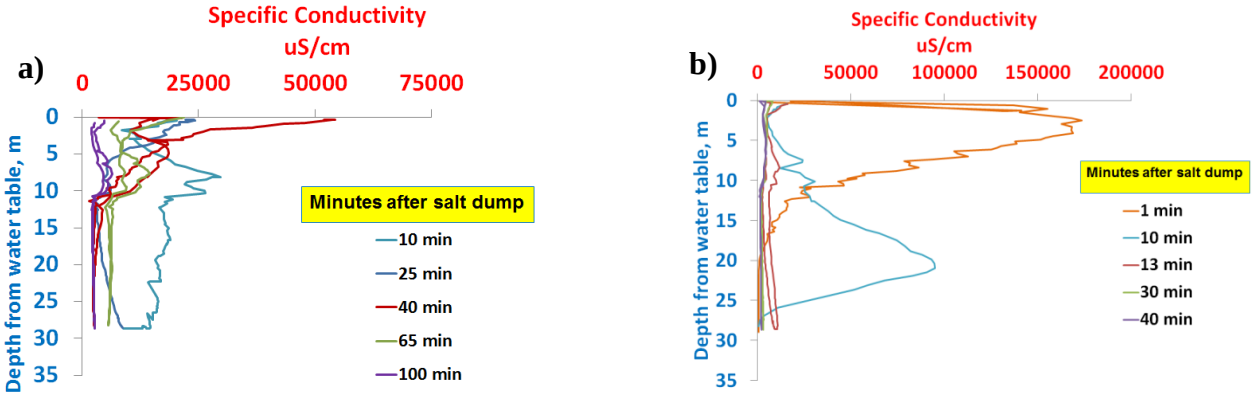

Fig. 24 Conductivity profile in PL10B, showing the slug moving to the bottom just after the dump (Table 3). Plot **(a)** shows the specific conductivity for PL10B in 18/07/13 and **(b)** in 19/07/13. Note *c.* 60% of the initial slug is vanished few minutes later.

The conductivity profiles from the travelling array could not be acquired in PL10E due to a blockage in the borehole caused by the permanent electrodes, which impede the use of the travelling array. As well the traveling array could not be used in PL10A due to distances restriction; the travelling electrode was not designed to cross the road and profile the borehole. For these reasons, there was no travelling electrode or conductivity data obtained for PL10A and PL10E during the latter two dumps.

Discussion:

In this work we present the results from field experiments held in the Chalk aquifer in Bottom Barn Abstraction in Berkshire UK. We demonstrate that it is possible to measure a streaming potential response to a pressure gradient in field conditions during a long-term pump and recovery test (i.e. drawdown and build up) in instrumented boreholes. These results suggest that the electrokinetic component of spontaneous potential can be successfully monitored and characterised in a borehole when a pressure gradient is induced, e.g. while injecting a fluid into the formation. Moreover, the value of the coupling coefficient of the streaming potential from the field experiment is similar to the coefficient obtained in the laboratory. The temperature effect over the borehole voltage measurements was present and could not be completely de-trended since the temperature probe was installed in a different position from the borehole electrode used for this analysis. Instead, moving averages was used to reduce the noise followed by a filtering stage to smooth the temperature effect. Surface electrodes did not measure any significant signal above background noise (*c.* 200 µV). This could be because surface electrodes were far from the signal generation. The slow response of voltage to pressure buildup is attributed to the inertial forces exerted over the fluid due to the large water pumping rates, where the fluid continues moving after the pump was turned off. This hypothesis is supported by the high

transmissivity values obtained in the characterisation of the field, deriving in high effective permeability which allows transmitting changes in pressures to the aquifer. This high transmissivity in the fracture network transmitted the momentum through the aquifer, i.e. water continued moving by inertia, generating a slow decay in the EK potential.

Despite the high initial concentrations measured in the salt dump boreholes, no conclusive EC voltage response was observed during the salt injection experiments. The peak of voltage measured by the surface electrodes in dumps I and II was related to a redox potential. This redox potential was generated thanks to the high salinity concentration at the top of the borehole in contact with the metallic casing in PL10A which, being transmitted to surface through the casing. The amplitude decline of the redox potential through the surface was estimated in 0.06mV m^{-1}. The redox potential decreased with the increasing distance from the dump borehole (i.e. PL10A). This value suggests that signal disappeared before reaching the monitoring wells, thus explaining why none of the borehole electrodes in PL10B or PL10E could measure any redox potential. The two last dumps (III and IV; table 3) in PL10B, which is completed with plastic casing, confirmed that the response measured in the dumps I and II was attributed to a redox potential. There was no conclusive electrochemical response during the final two salt dumps.

The conductivity profiles for PL10A suggest a higher hydraulic conductivity 10 meters below the water table, probably due to a higher fracture density. The conductivity profile in PL10E is different than profile in PL10B in the first three meters below the water table. The possible explanations for this includes an EK effect due to a crossflow near this depth, EC effect due to the apparent better connectivity through the fracture network and different groundwater composition. However, the pressure gradient that could be generated by the crossflow is very small, thus EK effect seems not feasible. The EC origin hypothesis seems unlikely since the separation of the curve can be seen in profiles made before the salt dump. The difference in groundwater composition can be only speculative, since no water composition measurements were done. Due to this we hypothesise that PL10A and PL10E could be connected through the fracture network. PL10B does not show any evidence of connectivity with the fracture network in the upper section of the borehole in ambient conditions; as well there is no evidence of an upflow, as in PL10A, thus explaining the contrasting conductivity patterns between PL10A and PL10B and the fast sinking of the brine slug in borehole PL10B (fig. 24a & 24b). The fast decrease of salt concentration in the aquifer, the time that it takes to the slug to travel until the neighboring boreholes and the non-apparent interconnection of wellbore PL10B within the fracture network are the possible reasons why the experiment did not provide the expected results.

The results obtained from streaming potential experiments suggest that EK potential can be successfully measured and characterised for water, steam or any displacement fluid injection in a hydrocarbon reservoir, allowing monitoring and characterising underground fluid flow to improve hydrocarbon production.

In the case of the EC potential an increase of NaCl mass poured into the borehole is advised. The numerical reservoir simulation proposed by Jackson *et al.* (2012b) suggests that a concentration as high as 1M would be needed to produce a measurable EC potential. As well, a denser pattern of measurement should be considered (e.g. a 360 degree electrode coverage around borehole) in order to identify the flow pattern around the borehole and increase the possibility of measuring a significant EC potential.

Conclusions:

This work presents the field experiment results from the experiments held in the Chalk aquifer in Bottom Barn Abstraction in Berkshire UK. The conclusions of the field experiments for EK and EC potentials are as following:

For EK potential:

1. A clear EK response was observed by borehole electrodes. The field coupling coefficient obtained is comparable to the coefficient obtained in laboratory test.
2. Surface array does not show evidence of EK potential. The distance between electrodes location and the depth of EK potential generation caused the dissipation of voltage signal before it reaches the electrodes.
3. Inertial effects originated by the large drawdown rates, causes the voltage to respond slower to pressure changes. The high effective permeability suggests that the water momentum (caused by inertia) was transmitted through the aquifer.
4. It is demonstrated that EK potential can be measured and characterised during long term pump and recovery test.

For EC potential:

1. No EC potential could be measured due to the small mass of salt injected; larger NaCl concentration in borehole (as high as 1M) is required to generate a significant voltage response.
2. Redox potential was generated and recorded only by the surface array in the first two dumps. This was attributed to the attenuation factor estimated in (0.06mV m^{-1}).
3. Conductivity profiles display a difference in patterns at 2 and 8 m for PL10E respect PL10B. The possible explanations for these are: **a)** A crossflow at 2 m deep in PL10E causes water to shear the mineral, thus transporting charges. The same could be occurring at 8 m deep for both boreholes. **b)** Different groundwater composition causes the occurrence of EC potential. However, due the lack of chemical tests this can be only hypothesised.

4. The fast decrease of conductivity in the injection borehole and the inexistent change in the conductivity in the monitoring wells during the experiment suggests that salt is dissipated before an EC signal could be measured.
5. Conductivity profile in PL10A suggests the existence of a high hydraulic conductivity region at the top of the well.
6. The fast displacement of the saline brine slug towards the bottom of borehole PL10B was observed in the conductivity profiles. This assumes that there is no upflow in PL10B and no apparent crossflow through the matrix.

The results of the EK experiment demonstrate that a proper EK coupling coefficient can be obtained and although is not totally analogous to other formations, it can be used to characterise EK signals; this signals can be applied to control systems in order to monitor and prevent water production during water (waterflooding) or steam injection (steamflooding). Reproduce these results in a producing oilfield and monitor waterflooding would be a next step to follow.

The results for the EC experiment suggests that a larger amount of salt shall be poured into the wellbore; as well a plastic casing wellbore has to be taken into consideration in order to prevent any possible masking of EC potential by redox potential. Future work will consider a larger concentration of salt (1M) in a different field site which allows the salt slug to reach crossflow areas and be transported to generate a salinity contrast, instead of being dispersed in a shallow fracture network or never reach a crossflow.

Nomenclature:

C_{EK} = Electrokinetic coupling coefficient, $VMPa^{-1}$
K = Absolute permeability, miliDarcys (mD)
∂V = Voltage (electrical potential) change
∂P = Pressure change
σ = Electrical conductivity with formation saturated with groundwater, Sm^{-1}
FF = Formation factor, dimensionless
Φ = Porosity (%)

References:

Bolève, A., Janod, F., Revil, A., et al. 2011. Localization and quantification of leakages in dams using time-lapse self-potential measurements associated with salt tracer injection. *Journal of Hydrology* **403** (3): 242-252. http://dx.doi.org/10.1016/j.jhydrol.2011.04.008

Braun, B.M. and Weingartner, H. 1985. Transference numbers of aqueous NaCl and Na_2SO_4 at 25 °C from EMF measurements with sodium selective glass electrodes. *Journal of Solution Chemistry* **14** (9): 675–686. http://dx.doi.org/10.1007/BF00646059

Burgess, J. 1978. *Metal Ions in Solution.* New York, Ellis Horwood.

Butler, A.P., Mathias, S.A., Gallagher, A.J., et al. 2009. Analysis of flow processes in fractured chalk under pumped and ambient conditions (UK). *Hydrogeology Journal* **17** (8): 1849-1858. http://dx.doi.org/10.1007/s10040-009-0477-4

Chen M.Y., Raghuraman, B., Bryant, I. 2006. Streaming Potential Applications in Oil Fields. Paper SPE 102106 presented at the SPE Annual Technology Conference and Exhibition, San Antonio, Texas, 24-27 September. http://dx.doi.org/10.2118/102106-MS

Corwin, R.F. and Hoover, B.H. 1979. The self-potential method in geothermal exploration. *Geophysics* **44** (2): 226-245. http://dx.doi.org/10.1190/1.1440964

Dake, L.P. 1978. *Fundamentals of Reservoir Engineering*. Elsevier, Amsterdam.

Darnet, M. and Marquis G. 2004. Monitoring reservoir fluid flow from surface self-potential (SP) measurements: application to geothermal reservoirs. Paper SEG 2004-1159 presented at the 2004 Annual Meeting, Denver, Colorado, 10-15 October.

Department of the Army. 1989. *Water Quality Analysis/Sets.* Engineer Technical Manual. Washington, D.C.: C-61

Deussen A. and Leonardon E. 1935. Electrical Exploration of Drill Holes. Paper API 35-047 presented at Fifth Mid-Year Meeting, Tulsa Oklahoma., 4 May.

Gulamali, M.Y., Leinov, E., Jackson, M.D. 2011. Self-potential anomalies induced by water injection into hydrocarbon reservoirs. *Geophysics* **76** (4): 283-292. http://dx.doi.org/10.1190/1.3596010.

Handreck, K.A., Black, N.D. 2005. *Growing Media for Ornamental Plants and Turf*. Third Edition. Sydney, University of New South Wales Press Ltd.

Hunt C. and Worthington, M.W. 2000. Borehole electrokinetic responses in fractured dominated hydraulically conductive zones. *Geophysical Research Letters* **27** (9): 1315-1318. http://dx.doi.org/10.1029/1999GL011099

Hunter, R.J. 1981. *Zeta Potential in Colloid Sciences: Principles and Applications* third edition. New York: Academic Press.

Jaafar, M.Z., Vinogradov, J., Jackson, M.D. et al. 2009. Measurements of Streaming Potential for Downhole Monitoring in Intelligent Wells. Paper SPE 120460 presented at the SPE Middle East Oil & Gas Show and Conference, Bahrain, 15-18 March.

Jackson, M.D., Vinogradov, J., Saunders, J.H. et al. 2011. Laboratory Measurement and Numerical Modelling of Streaming Potential for Downhole Monitoring in Intelligent wells. *SPE Journal* **16**: 625-636, ISSN: 1086-055X.

Jackson, M.D., Gulamali M.Y., Leinov, E., et al. 2012b. Spontaneous Potentials in Hydrocarbon Reservoirs During Waterflooding: Application to Water-Front Monitoring. *SPE Journal* **17** (1): 53-69. SPE-135146-PA. http://dx.doi.org/10.2118/135146-PA

Jackson, M.D., Butler, A.P., Vinogradov, J. 2012a. Measurements of spontaneous potential in chalk with application to aquifer characterization in the southern UK. *Quarterly Journal of Engineering Geology and Hydrogeology* **45**: 457-471. http://dx.doi.org/10.1144/qjegh2011-021

Javadi, A.A. and Abd-Elhamid, H.F., 2011. A simulation-optimization model to control seawater intrusion in coastal aquifers using abstraction/recharge wells. *International Journey for Numerical and Analytical Methods in Geomechanics* **36** (16): 1757-1779. DOI 10.1002/nag.1068.

Johnson, H.M. 1962. A History of Well Logging. *Geophysics* **27** (4): 507-527. http://dx.doi.org/10.1190/1.1439054

Jones, H.K., and Robins, N.S. 1999. *National Groundwater Survey. The Chalk Aquifer of the South Downs.* Keyworth Nottingham, NERC, BGS.

Jouniaux, L.A., Maineault, A., Naudet, V. et al. 2009: Review of Self-potential methods in Hydrogeophysics. *C.R. Geoscience* **341** (10-11): 928-936. http://dx.doi.org/10.1016/j.crte.2009.08.008

Kendall, H.A. 1965. Application of SP Curves to Corrosion Detection. *Journal of Petroleum Technology* **17** (9): P. 1029-1032. DOI 10.2118/1065-PA.

Kostic, M.B., Radakovic, Z.R., Radovanovic, N.S., et al. 1999. Improvement of electrical properties of grounding loops by using bentonite and waste drilling mud. *IEE Proceedings, Generation, Transmission and Distribution* **146** (1): 1-6. http://dx.doi.org/10.1049/ip-gtd:19990057

Lenntech BV. 1993. Water Treatment Solutions. http://www.lenntech.com/.

MacDonald, A.M. and Allen, D.J. 2001. Aquifer properties of the Chalk of England. *Quarterly Journal of Engineering Geology and Hydrogeology* **34** (4): 371-384. http://dx.doi.org/10.1144/qjegh.34.4.371

Marshall, D.J. and Madden, T.R. 1959. Induced polarization, a study of its causes. *Geophysics* **24** (4): 790-816. http://dx.doi.org/10.1190/1.1438659

Mathias, S.A., Butler, A.P., Peach, D.W., et al. 2007. Recovering tracer test input function from fluid electrical conductivity logging in fractured porous rocks. *Water Resources Research* **43** (7): n/a-n/a. http://dx.doi.org/10.1029/2006WR005455

MATLAB®, Version R2012a (7.14). 2012. US: The Mathworks, Inc.

Meier, P.M., Carrera, J., Sanchez-Vila, X. 1998. An evaluation of Jacob's method for the interpretation of pumping tests in heterogeneous formations. *Water Resources Research* **34** (5): 1011-1025. http://dx.doi.org/10.1029/98WR00008

Moore, H. 2013. *MATLAB for engineers*, third edition. London, Pearson.

Mounce W.D. and Rust W.M. 1944. Natural Potentials in Well Logging. *Transactions* AIME **155** (1): 49-57. DOI 10.2118/944049-G.

Oosterbaan, R.J. and Nijland, H.J. 1994. *Determining the Saturated Hydraulic Conductivity, Chapter 12 in: Ritzema H.P.(Ed), Drainage Principles and Applications. ILRI* **16 (**2), Wageningen, The Netherlands.

Ortiz, I. Jr., Von Goten, W.D., Osoba, J.S. 1972. Relationship of the Electrochemical Potential of Porous Media with Hydrocarbon Saturation. *The Log Analyst* (3-4): 25-32.

Perrier, F. and Pant S.R. 2005. Noise Reduction in Long-term Self-potential Monitoring with Travelling Electrode Referencing. *Pure and Applied Geophysics* **162** (1): 165-179. DOI 10.1007/s00024-004-2585-3.

Price, M. 1987. Fluid flow in the Chalk of England. Edit.by Goff, J.C. & Williams, B.P.J. *Fluid Flow in Sedimentary Basins and Aquifers*. Geological Society, London, Special Publications **34.** 141–156.

Revil, A. 1999. Ionic Diffusivity, Electrical Conductivity, Membrane and Thermoelectric Potentials in Colloids and Granular Porous Media: A Unified Model. *Journal of Colloid and Interface Science* **212** (2): 503-522. http://dx.doi.org/10.1006/jcis.1998.6077

Saunders, J.H., Jackson, M.D., Pain, C. 2006. A new numerical model of electrokinetic potential response during hydrocarbon recovery. *Geophysics Research Letters* **33** (15). DOI: 10.1029/2006GL026835.

Saunders, J.H., Jackson, M.D., Pain, C.C. 2008. Fluid Flow Monitoring in Oil Fields Using Downhole Measurements of Electrokinetic Potential. *Geophysics* **73** (5). DOI: 10.1190/1.2959139.

Schurch, M., and Buckley, D. 2002. Integrating geophysical and hydrochemical borehole-log measurements to characterize the Chalk aquifer, Berkshire, United Kingdom. *Hydrogeology Journal* **10** (6): 610-627. http://dx.doi.org/10.1007/s10040-002-0220-x

Shook, M., Li, D., Lake, L.W. 1992. Scaling Immiscible Flow through Permeable Media by Inspectional Analysis. *In-Situ* **16** (4): 311-350.

Sill, W.R. 1983. Self-potential modeling from primary flows. *Geophysics* **48** (1), 76-86. doi: 10.1190/1.1441409

Silvion reference electrodes for cathodic protection. Silvion Limited. Lincolnshire, UK. www.silvion.co.uk.

Sinnott, R.K., 2005. *Chemical Engineering Design*, fourth edition. London, Elsevier.

Tasaka, M., Morita, S., Nagasawa, M. 1965. Membrane potential in nonisothermal systems. *Journal of Physical Chemistry* **69** (12): 4191-4197. http://dx.doi.org/10.1021/j100782a021

Wheater, H.S., Peach, D.W. 2004. Developing interdisciplinary science for integrated catchment management: The UK LOwland CAtchment Research (LOCAR) Programme. *International Journal of Water Resources Development* **20** (3): 369-385. http://dx.doi.org/10.1080/0790062042000248565

White, HJO. 1907. *The Geology of the Country Around Hungenford and Newbury*. Memoir, British Geological Survey, Keyworth, UK.

Williams, A., Bloomfield, J., Griffiths, K., et al. 2006. Characterising the vertical variations in aquifer properties within the Chalk aquifer. *Journal of Hydrology* **330** (1-2): 53–62. http://dx.doi.org/10.1016/j.jhydrol.2006.04.036

Wyllie, M.R.J. 1949. A quantitative analysis of the electrochemical component of the S.P. curve. *Transactions* AIME **1 (**1): 17-26. http://dx.doi.org/10.2118/949017-G

Wyllie, M.R.J. 1951. An investigation of the electrokinetic component of the self-potential curve. *Transactions* AIME **3** (1): 1-18. http://dx.doi.org/10.2118/951001-G

APPENDIX A - Literature review

Org. /Publication	Year	Title	Authors	Contribution/Milestone
SPE/API 35-047	1935	Electrical Exploration of Drill Holes	Alexander Deuseen; Eugene G. Leonardson, Schlumberger	First paper in recognising the Electrochemical potential as an important component of the self-potential (SP) curve. Streaming potential just makes small contributions, sometimes negligible.
SPE/AIME 944049	1943	Natural Potential in Well Logging	W.D. Mounce and W.M. Rust, JR	First characterisation of seat conditions for electrochemical potential occurrence. (Shale)Such characterisations were similar to conditions existed in field.
SPE 949017	1949	A Quantitative Analysis of the Electrochemical Component of the S.P. Curve.	M.R.J. Wyllie	First providing quantitative, reproducible laboratory and field results of the electrochemical component of the SP.
Transactions AIME Vol. 1 No. 1. Pages: 17-26	1951	An investigation of the eletrokinetic component of the self-potential curve.	M.R.J. Wyllie	First establishing a relationship for streaming potential from laboratory tests using laboratory prepared and field aqueous muds. In Field experiments demonstrate that the algebraic sum of electrochemical and streaming potentials yields the SP potential.
SPWLA 1973-vXIVn2a3	1973	Relationship Of the Electrochemical Potential of Porous Media with Hydrocarbon Saturation	Isaias Ortiz Jr., W.D. Von Gonten J.S. Osoba	First characterisation of electrochemical response with variations in hydrocarbon saturation and measurement of potential on samples from formations with different content of shale.
Hydrogeology Journal Vol. 17 No. 8. Pages 1849-1858	1999	Analysis of flow processes in fractured chalk under pumped and ambient conditions (UK)	A.P. Butler S.A. Mathias A.J. Gallagher D.W. Peach A.T. Williams	Characterisation of geophysical properties of the formation in Bottom Barn Abstraction, Berkshire UK in pumping conditions (for one of the six wells drilled) and in ambient conditions (for two wells).
SPE 120460	2009	Measurement of Streaming Potential for Downhole Monitoring in Intelligent Wells.	M.Z. Jaafar J. Vinogradov M.D. Jackson J.H. Saunders C.C. Pain	Provide laboratory measurements of streaming potential coupling coefficients performing an experiment which consist in a sst core subject to a pressure gradient, making a brine to pass through this core and measure the voltage produced. Explanation of the methodology to reach the model. Also demonstrates that at salinities far above the sea salinity, streaming potential signals can be effectively measured.
GEOPHYSICS Vol. 76 No. 4	2011	Self-Potential Anomalies Induced by Water Injection into Hydrocarbon Reservoirs	M.Y. Gulamali E. Leinov M.D. Jackson	Numerical simulation of hydrocarbon reservoir to compare EK, EC and TE components of SP signal, characterising the response at different timeline before water breakthrough and with different brine saturation.
SPE 135146	2012b	Spontaneous Potential in Hydrocarbon Reservoirs During Waterflooding: Application to a Water-Front Monitoring.	M.D. Jackson, M.Y. Gulamali, E. Leinov, J.H. Saunders, J. Vinogradov	First having usable results from numerical modelling to characterise electrokinetic, electrochemical and thermoelectric potential to monitor water front.
Quarterly Journal of Engineering Geology and Hydrogeology Nov. 2012 Vol. 45 (p. 457-471)	2012a	Measurements of spontaneous potential in chalk with application to aquifer characterisation in the southern UK.	M.D. Jackson, A.P. Butler & J. Vinogradov	First measurements of EK potential coupling coefficients in chalk samples saturated with natural groundwater. Preliminary Field measurements of spontaneous potential at ambient and pumped condition in Chalk aquifer.

SPE/API 35-047

Electric Exploration of Drill Holes (1935)

Authors: Alexander Deussen, Eugene G. Leonardson, Schlumberger.

Contribution to SP Signal understanding:
This paper is the first one explaining how the spontaneous potential is achieved together with its applications to reservoir characterisation. It also mentions the Electrochemical Potential effect on the Spontaneous Potential (SP) response, and it contribution as an important component of this signal.

Objective of the paper:
To explain the principles of electrical logging (resistivity and SP at the time) in drilled holes and it applications in oil reservoir characterisation.

Methodology:
Theoretical explanation of the principles on electrical signals in rocks, resistivity measurements in a drill hole, Spontaneous Potential and how these signals behave in formations in order to properly interpret them in a log. This theory is backed up with real logs, methodology and examples from the field. This paper recognises the importance of the electrochemical potential in the SP section.

Conclusion reached:
The contribution of electrical logging constitutes a new way of characterising reservoirs in drilled holes. With this, we can know certainly the production horizon and save money making coring not entirely necessary. Also mentions that the only trustable and economical way to obtain full information from a well is through electrical logging, making it even better than drill cutting and coring analysis.

Comments:
This paper contains the basis to understand the importance of electrical logging. Nevertheless, what is more interesting to this project is the mentioning of the Spontaneous Potential study and the electrochemical potential reference as a consequence of electrolytes that are in contact (electro-osmosis).

SPE/AIME 944049

Natural Potential in Well Logging (1943)

Authors: W.D. Mounce, W.M. Rust Jr.

Contributions to SP signal understanding:
Mounce & Roust were the first to make a characterisation of electrochemical potential occurrence in certain conditions, using shale as main porous media. These conditions were designed to recreate the field environment.

Objective of the paper:
To examine the physics and explain with fundaments and experiments with shale cores, the universally accepted electrical logging practices.

Methodology:
Performing experimental results using shale cores with fresh-water, shale and salt-water. Firstly the characterisation was performed to explain the electrofiltration potential (streaming potential). With the results, the necessity of performing further experiments characterising the response with shale cores, propitiating the understanding of the electrochemical potential.

Conclusion reached:
The results of the experiments reached to the understanding of the Electrofiltration and Electrochemical (EC). It is stated that the EC is the main contributor to the SP signal and a relationship is established.
$E = k \log CdC. = k(\log C1 - \log C2)$ where E is the potential, K is a constant depending the nature of electrolyte and C_1 and C_2 the concentration of each electrolyte.

Nevertheless, the paper comprises that this theory is not entirely true since the electrode is in contact with the drilling mud and being this almost entirely homogeneous, the only way a difference in potential can occur is with a current flowing in the mud. Then, it is clear that the SP signal generated is due to the contrast in the salinity of the mud and the formation fluid.

Comment:
This paper is the first that establishes a characterisation of the EC component of the SP signal in an experiment comprising a shale core and brines of different salinities. Also, these experiments are the first ones estimating that the EC potential is the main contributor to the SP signal.

SPE 949017
A Quantitative Analysis of the Electrochemical Component of the SP Curve. (1949)

Authors: M.R.J. Wyllie.

Contributions to SP signal understanding:
This paper is the first providing quantitative, reproducible results from laboratory and field experiments for EC potential characterisation of the SP signal.

Objective of the paper:
To propose a relationship from laboratory and field experiments, in order to quantitatively analyse the electrochemical component of the SP curve.

Methodology:
This paper provides a theoretical analysis of the experiments carried out by Mounce and Rust (1943), proposing correlations for the boundary potentials from the expression of Henderson (1907) for dilute solutions. Later this is taken to laboratory experiments using two different samples of shale previously air dried, and setting them up with Hg/Hg_2Cl_2 electrodes. For these experiments a brine of NaCl with different concentrations was used. Several methods were used for satisfactorily bring sodium chloride in contact with the shale surfaces, but there was one particularly effective. This consists of cementing a flanged 24/40 male glass taper to the shale by means of a mixture comprising 100 grs of green optical pitch and 1 cc. of oil. Glass tubes in L-shape glass are then fitted to the standard tapers to hold the NaCl solutions. For the field experiments, generally logs were obtained using three different mud resistivities which were altered by the salt content. The logs reflect the effect of the shale in the SP signal (which main contributor is the EC). The results obtained were normalised to a temperature of 64.4 F for a fair comparison.

Conclusion reached:
The analysis of the effects of shale in the EC component of the SP can be seen in both, laboratory and field experiments. Nevertheless, the results were only for two shale samples, thus the possibility of finding different results was latent at the time the paper was written. Also, the concentrations used represent molarities outside the range for which most electrochemical characterisations have been made. This means that the results will only be approximations when generally applying to log data. Despite this apparent inaccuracy, these errors won't totally discard the results.

Comment:
This paper contributes with the first characterisation from laboratory and field experiments for Electrochemical potential in a shale environment. It is important to mention that the results, despite not totally accurate, were successfully applied to determine that shale can have electrochemical properties. The experiment methodology and the results were the central part of this paper and the most contributors to my understanding of SP.

SPE 951001. *Transactions* AIME Vol. 1 No. 1. Pages: 17-26

An investigation of the electrokinetic component of the self-potential curve. (1951)

Authors: M.R.J. Wyllie.

Contributions to SP signal understanding:
First establishing a relationship for streaming potential from laboratory tests using laboratory prepared and field aqueous muds. In Field experiments demonstrated that the algebraic sum of electrochemical and streaming potentials constitutes the SP potential.

Objective of the paper:
The objective of this paper is to validate previous quantitative analysis of SP in previous paper by Wyllie (1949) with experiments held in a streaming potential cell with multiple fluid samples as well as field tests with the same mud samples used in laboratory.

Methodology:
A streaming potential cell was used together with several mud samples in order to typify the results obtained. The SP cell has an arrangement of calomel electrodes. Muds, which have similar resistivity to the presented by the connate water, are put inside and subject to pressure through a filter paper and to high temperature tests. Plots of total filtrate versus pressure were obtained. The temperature of the calomel electrodes has to remain the same in order to prevent a drift in the measurement of the potential generated. The field experiment consisted in characterization of core samples. Then increases of pressure were held in the borehole, which transmitted the pressure change to the mud. The characterizations provide a probe of the influence in temperature on streaming potential as well as the influence of pressure in the same streaming potential.

Conclusion reached:
The different muds tested yielded a typical response of SP potential with the increase of pressure at any temperature. However, the effect of the temperature on the SP results was also observed despite they were small.

Comments:
This paper is the first which provides an expression to describe the SP potential validated by laboratory and field tests. The contribution of this paper to my project is related to the responses observed in SP to the pressure gradient in muds with different characteristics but with resistivity close to the formation water. This was a key finding since the experiment was held in a chalk aquifer with fresh formation water. It is important to note that temperature alterations, although small, were already acknowledged.

SPWLA 1973-vXIVn2a3

Relationship of the Electrochemical Potential of Porous Media with Hydrocarbon Saturation. (1973)

Authors: Isaias Ortiz Jr, W.D. Von Gonten, J.S. Osoba

Contributions to SP signal understanding:
This paper provides the first characterisation of electrochemical (EC) response with different hydrocarbon saturation and measurement of the potential on samples from formations with different shale content.

Objective of the paper:
The objective of this paper is to evaluate the changes in the electrochemical potential with varying hydrocarbon saturation in a porous media, and relate this change to cation exchange capacity.

Methodology:
Seventeen samples were to be used as porous media and varied from clean sands to shaly sands being obtained from 10 different formations. The samples were 1.5 inches in diameter and 1.75 inches length. Then cores were dried and then saturated with brine. Plugs were inserted in Hassler holder separating two tanks with different brine salinity. Silver-Silver chloride electrodes connected to a voltimeter were placed in each solution and the actual potential was measured. Later, the electrodes were interchanged. An average was taken as the average potential across the core. Samples were then desaturated to a establish water saturation and paraffin was injected. Different paraffin saturation was established for each sample. After this, actual potential measurements were taken. Water and hydrocarbon saturations were determined with USBM extraction apparatus containing toluene.

Conclusion reached:
The increasing hydrocarbon saturation supresses SP and as the water saturation in the core is decreased, actual potential in the sample is near that of the perfect membrane.
The hypothesis of Hill and Millburn and Smits were proven in laboratory conditions as the effective concentration of exchange ions in oil bearing sands is increased. The modified Smits equation satisfactorily represents the laboratory results.

Comment:
This paper is explaining the proper steps for a laboratory experiment to characterise the electrochemical potential with variable hydrocarbon saturation in samples going from virtually clear sands to shaly sands. This provides the important information on how the increasing hydrocarbon saturation supresses the SP potential and how decreasing water saturation leads the actual potential to be close to a prefect membrane.

Hydrogeology Journal Vol. 17 No. 8 (P. 1849-1858)

Analysis of flow processes in fractured chalk under pumped and ambient conditions (UK) 1999

Author: A.P. Butler, S.A. Mathias, A.J. Gallagher, D.W. Peach, A.T. Williams

Contributions to SP signal understanding:
This paper contributes with the characterisation of the geophysical properties of the Bottom Barn Abstraction in Berkshire, UK in pumped and ambient conditions. It provides important information (e.g. gamma ray log, conductivity, density fracture and it dip angle, hydraulic conductivity, etc.). Also states the location of the site and rough location of the boreholes used in this dissertation.

Objective of the paper:
To characterise geophysical properties of the location under pumping and ambient conditions, in order to improve the parameters previously obtained and use them in groundwater models of water-resources sites.

Methodology:
The methodology included several tests to characterise the flow patterns in the formation. The study begins with a lithostratigraphy review and shows a summary of the geophysical properties (gamma ray log, diameter of the boreholes or caliper, fracture orientation and hydraulic conductivity. Following describes the results obtained by an optical televiewer (borehole imaging) to provide the input data to calculate the fracture dip angle. A packer test is held and water is pumped out until steady-state drawdown to derive hydraulic conductivity. After all this is acquired, a pumping test is done to estimate effective transmissivity using Jacob's method assuming aquifer is homogeneous and isotropic. In order to characterise the upflow in the borehole, a flow logging log with an impeller and a heat-pulse flowmeter is done. Finally a dilution test is performed to acquire flow horizons. For this a conductivity probe is used.

Conclusion reached:
The tests explained in this paper provided new data regarding the flow patterns in the aquifer (BBA). In ambient conditions the system behaviour was difficult to establish. However, during pumping conditions the flow could be easily characterised. A significant crossflow was concluded in certain regions. The transmissivity estimated showed a difference in values attributed to the non-linear head losses caused by turbulence and inertial effects. The changes in well flow profiles when flow is induced by pumping stage are due to changes in head distribution of the large scale flowpaths.

Comments:
The information contained in this paper was essential to understand the results of the experiment described in this work. Thanks to the profiles and the data contained in this document, a series of conclusions could be reached. The crossflow patterns, the transmissivity of the formation and all the geophysical data provides a clear insight of the formation properties and flow behaviour in the aquifer.

SPE 120460

Measurement of Streaming Potential for Downhole Monitoring in Intelligent Wells. (2009)

Author: M.Z. Jaafar, J. Vinogradov, M.D. Jackson, J.H. Saunders, C.C. Pain.

Contributions to SP signal understanding:
This paper contributes with the first experimental measurements of the streaming potential coupling coefficient in NaCl saturated sandstones (above sea water saturation) They also provide new experimental data to be applied to numerical models in order to predict the signal of SP that would be generated in a production well. Also they confirm that the value of the electrokinetic coupling coefficient is lower with the increase in salinity, down to zero at seawater salinity.
Objective of the paper:
To present the first measured values of streaming potential and new experimental data and methodology for SP measurement.

Methodology:
The methodology consisted in pumping brine across a sandstone core, using synthetic oil as a hydraulic fluid. This pumping stage is done at constant rate to provide accuracy. The oil used allows capturing air bubbles in the brine and prevents the corrosion of the pump. Pressure differences across the core sample are measured using pressure transducers, and voltage is measured through the sample using four Ag/AgCl non-polarizing electrodes. Two of the electrodes are positioned out of the flow path to eliminate potential variations and electrode effects. The other two are located at each face of the core sample inside the pressure vessel. All the experiment set was provided with a Faraday cage properly grounded. This Faraday cage provides protection against spurious external noise. Two rock samples were used from the same outcrop. One of the samples was sectioned parallel to bedding and the other one perpendicularly. Varying brine salinity is pumped through the core sample at a constant flow rate, until a stable pressure and voltage difference is recorded through the core. Conductivity was also measured to characterise EC potential generation. A numerical model was used to simulate the streaming potential during waterflooding and evaluate the impact of brine salinity and reservoir permeability heterogeneity.

Conclusion reached:
The streaming potential measured in a sandstone core sample saturated with different values of NaCl provides a value despite the value of salinity. This suggests that the monitoring of underground flow can be achieved. Numerical model provides and insight of the magnitude of the streaming potential that would be measured by downhole electrodes. This potential can be measured from tens to hundreds of meters before it reaches the wellbore region.

Comments:
This paper was useful to understand the use of non-polarizing electrodes to acquire voltage measurements. Also, it has a very good explanation of how the data gathered in the laboratory test can be used as an input for reservoir numerical model purposes and to simulate the potential that will be generated with the inflow of water in a hydrocarbon reservoir. Also the model results demonstrate that the incoming fluid will generate a sufficient streaming potential to be measured from up to hundreds of meters away.

Geophysics Vol. 76 No. 4

Self-Potential Anomalies Induced by Water Injection into Hydrocarbon Reservoirs. (2011)

Authors: M.Y. Gulamali, E. Leinov, M.D. Jackson

Contributions to SP understanding:
This paper provides an excellent comparison between EK, EC and TE components of SP signal in a numerical simulation of hydrocarbon reservoir assessing the contribution of each potential to the overall SP signal. Also it characterises the response at different timeline before water breakthrough and with different brine saturation, thus providing more information for waterflooding monitoring characterization.

Objective of the paper:
To characterize (e.g. obtain coupling coefficients) the self-potential components of electrochemical, electrokinetic and thermoelectric potentials in a numeric model of a reservoir. This will help to understand how the potentials vary with the injection of fluids with different characteristics of salinity, temperature and pressure.

Methodology:
The Eclipse 100 black oil simulator was used to solve equations multiphase flow equations in 3D porous media. This simulator uses a finite-difference, finite-volume scheme to solve implicitly for the saturations, pressures, temperatures and salinities of each fluid phase, given the material properties of the medium and fluids. The model is based on Saunders *et al.*(2008) related to the flow of a wetting phase and an immiscible no wetting phase (Water and oil respectively) through a hydrocarbon reservoir. The reservoir consisted of an 1150 x 500 x 100 m sandstone reservoir constrained on three of its four sides by 50 m wide shales. The fourth side is bounded by 800 m of sandstone with same reservoir properties and fluid saturation. Transport of heat and salt is exclusively by advection. Advection dominates over diffusive processes. The 3D model is based on Saunders and discretized on a regular hexahedral mesh that is refined around the production well to allow determination of flow variables accurately. Initial conditions: Swc=1, So = 1. A colder, less saline fluid is injected at left-hand face of the reservoir at 10000 bbl/d. No capillary and gravity effects were taken into consideration, only viscous forces. Additional terms have to be added to describe EC and TE which were neglected.

Conclusion reached:
Under certain conditions of concentration injection (0.5M) an EK potential is at maximum at the saturation front. EC and TE is also generated but TE is small at the production well until after breakthrough. EC is relatively large and salinity front follows the saturation front. In this simulation, EC was contributing with 60% of the overall SP potential measured at the well. However, EK contributes more to measured SP at 200 days before water breakthrough. The results suggest that EK and EC effects need to be taken into consideration. TE can be discarded. For high saline or fresh formation brine, the overall SP signal may be used to detect an advancing waterfront in the production well.

SPE 135146. *SPE Journal* 17 (1): 53-69

Spontaneous Potential in Hydrocarbon Reservoirs During Waterflooding: Application to a Water-Front Monitoring (2012b)

Authors: M.D. Jackson, M.Y. Gulamali, E. Leinov, J.H. Saunders, J. Vinogradov.

Contribution to SP understanding:
They generated proper result from numerical modeling to characterise electrokinetic, electrochemical and thermoelectric potential. This will allow monitoring of the water front during flooding operations.

Objective of the paper:
To quantify the magnitude of the EC, EK and TE components of the SP during waterflooding operations. Also, to determine whether and under what reservoir and production conditions, the resulting SP will be enough to be detected. As well, to investigate is the measurements of SP in the boreholes can be used to monitor the advance of the waterfronts.

Methodology
This paper describes the use of a 3D numerical reservoir model where the horizontal sandstone reservoir layer has a vertical production borehole. The shale zones contained in the reservoir are water saturated, thus are conductive. The potential in the boundaries are used as a reference and represent the electrodes that would be placed at the surface. Porosity varies with the layers; permeability is zero so flow is not existent; flow is dominated by pressure gradients. The viscosities where chosen to create a shock-front-dominated displacement of oil by water. The coupling coefficients were also defined according previous experimental data. The governing equations are solved using Eclipse 100 black oil model. The following assumptions where made:

- Only water phase in the reservoir gives raise to SP (HC = non polar)
- Transport of heat and chemical species is dominated by advection.
- Interactions between fluxes other than those resulting from charges separations are negligible.
- Water is the wetting phase, oil is the non-wetting phase.
- Exposed reservoir layer is homogeneous.
- No gas is present
- Flow is only dominated by viscous forces, neglecting gravity and capillary forces.

The initial simulating case assumes a production of 10,000 bbl/d with brine flowing into the reservoir at the same rate. This brine has a salinity of 0.5M; reservoir permeability is uniform (150 mD) and initial formation temperature and formation-brine salinity are 80^{o}C and 1M respectively. These parameters simulate the injection of brine into a formation with saline-formation brine.

Conclusions achieved
The numerical modelling results suggest that the magnitude of the SP generated can be as large as hundreds of mV. Thus the encroaching water can be detected before it arrives to the production well. Before water breakthrough, SP at the well is dominated by EK and EC components generated from the gradients in fluid salinity and pressure.

Comments:
The results of this paper encourage a field experiment in order to better understand the components of the SP potentials so they can be applied to real reservoirs. This field experiment will validate the observations made here.

Quarterly Journal of Engineering Geology and Hydrogeology Vol. 45 (9): Pages 457-471.

Measurements of Spontaneous Potential in Chalk with Application to Aquifer Characterization in the Southern UK. (2012)

Authors: M.D. Jackson, A.P. Butler & J. Vinogradov.

Contribution to SP understanding:
This paper reports the first measurements of EK potential coupling coefficients in chalk samples saturated with natural groundwater as well as the preliminary field measurements of spontaneous potential at ambient and pumped condition in Chalk aquifer.

Objective of the paper
To know if SP monitoring can be used to characterise aquifer properties and groundwater flow in the UK chalk aquifer and provide a valuable additional dataset to complement borehole methods. The aim of the laboratory test is to measure the streaming potential coupling coefficient in chalk samples saturated with natural groundwater. All this will define if SP measurements can be used to detect and monitor groundwater flow in the UK chalk aquifer together with borehole data.

Methodology:
The laboratory experiment comprised a chalk sample from an outcrop of the Seaford Chalk. This sample was tightly confined in an acrylic pressure vessel. Hydrogen was used as confining fluid. The vessel is enclosed by a Faraday cage-like wrap made of foil. A syringe induces a fluid pressure difference across the plug. Again, as per Gulamali *et al.* (2011) synthetic oil is used as a hydraulic fluid to drive the water from the inlet to the outlet reservoir. Electrodes are placed out of the flow path in a brine reservoir that is in electrical contact with the water flow.

In the case of the field experiment, surface and borehole electrodes were used to measure the SP in ambient and pumping conditions in the Barn Abstraction in Berkshire, UK. The borehole electrodes were comprised in a borehole tool. The pump used to generate the pressure gradient was installed in another well connected to the aquifer. An extra reference electrode installed far away from the experiment zone was used to compare with the data collected by the surface and borehole arrays. The borehole tool was lowered to catch the crossflow during previous pumping experiments according to Butler *et al.* (2009). The pump is started and the datalogger will register all the measurements during this stage. Pump was suddenly stopped and pressure build up is expected. Then the response to the pressure change will be recorded by the datalogger.

Conclusion reached:
The possibility that the voltage variations observed are from electrokinetic origin is feasible. This comes from the observations of the water levels varying during pumping and ambient conditions, suggesting that temporal and spatial gradients in water pressure are present at ambient conditions. A 3D model that describes the local variations in water pressure and electrical resistivity is proposed. The laboratory measurements reported demonstrate that is possible to observe a negative value of the streaming potential coupling coefficient in a chalk sample saturated with groundwater. The field results are consistent with laboratory results observing small positive changes in the SP in response to the pressure drawdown and small negative changes in SP during pressure build up. However, since the SP signals induced by the changes in head were close to the background noise.

Comments:
This paper is the precursor of the experiments here described. The information contained in this paper was critical to establish the similarity between the coupling coefficient from laboratory experiments and the coupling coefficient from the field pumping experiment held in the following months after the publication of this paper. I consider this document one of the most important source of information regarding the experiments held in Bottom Barn Abstraction, Berkshire UK.

APPENDIX B

Mass Calculation of NaCl to achieve desired molarity in the borehole.

The calculation of the NaCl mass was done according to the desired molarity. The molarity for this experiment has to be representative of the molarity of the seawater in the English Channel, which is near 0.5 M or 35 gr/L. However, in order to comply with the Environmental Agency permit stipulation in the experiment site, a third of the seawater was specified. To calculate the mass to be thrown in the boreholes for the execution of the electrochemical experiment, we need to refer to caliper measurement (fig. B) to get an approximate of the volume of the borehole. The volume calculation was based on the average diameter of borehole PL10A, which is the original well designated for the brine injection. According to Butler *et al.* (2009) the average value of diameter is 0.206 m, and having into consideration the water table of 90.45 m AOD measured recently with a dipper, then we can calculate the volume as explained below. With the molar mass of NaCl (58.44 gr/mol), and the volume then we can calculate the necessary mass.

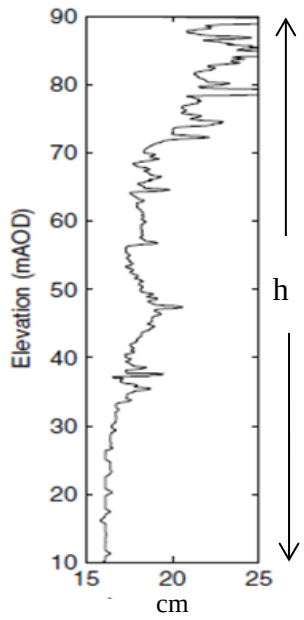

Fig. B-1 Caliper borehole measurement of diameter in cm.

$V = \pi h D^2 / 4$
where :
h : Depth of borehole from water table (m) = 90.5 m
D : Averaged borehole diameter (m) = 0.206 m
V : Volume of water in borehole (m^3).
estimated volume V = 3.014 m^3 or = 3014 Liter

With the volume in the borehole then we can calculate the mass of NaCl required:

Molar mass NaCl = 58.44 gr mol^{-1}
Mol required (1/3 sea water salinity) = 0.17 Mol
Mass required per liter = 9.93 gr/L
Total mass required = 28200 gr. = 28.2 Kg NaCl total.

The first salt dump was produced with salt dissolved in water. The amounts were carefully approximated to prevent water saturation. The solubility of NaCl in water at 25°C is of 360 gr/L. In the experiment we dissolved 31.5 Kg of NaCl in 150 L of tap water. This gives an approximate solubility of 210 gr/L. The molarity reached in the borehole overall then is:

Total amount of water in water (approx.) in liter = 3014 + 150 = 3164 L.
Total amount of NaCl dissolved = 31.5 Kg or 31500 gr.
Estimated molarity : 9.95 gr/L. or 0.17 Mol.

This complies with the desired initial concentration. It is important to note that the salt concentration of the tap water was not taken into consideration.

The following salt dumps were done in solid state directly to the borehole. The molarity was approximated as per the process previously described. Table B-1 shows the approximated concentrations of all the salt dumps:

Table B-1: Salt dump locations, dates, mass and estimated concentrations

Salt Dump	Borehole	NaCl mass, Kg.	Mol concentration (gr/L)
1.- 16/07/13	PL10A	31.5 Kg. (dissolved)	9.95
2.- 17/07/13	PL10A	18.5 Kg. (Solid state)	6.1
3.- 18/07/13	PL10B	19.5 Kg. (Solid state)	6.5
4.- 19/07/13	PL10B	25 Kg. (Solid state	8.3

APPENDIX C

Signal treatment of Electrokinetic raw measurements.

The data acquired was in spreadsheets with different acquisition time steps going from one second, 5 seconds, one minute until 5 minutes. Thanks to the amount of data acquired (approximately 15 days) and that the rates were obtained in time steps of 5 minutes, it was decided to use this period of time. All the spreadsheets were passed under a careful scrutiny and the data points corresponding to five minutes period were selected, this included pressure and voltage from borehole PL10B (BE1 and BE2). This led us to have the first raw measurements accurately organised and ready for processing (Fig. C-1).

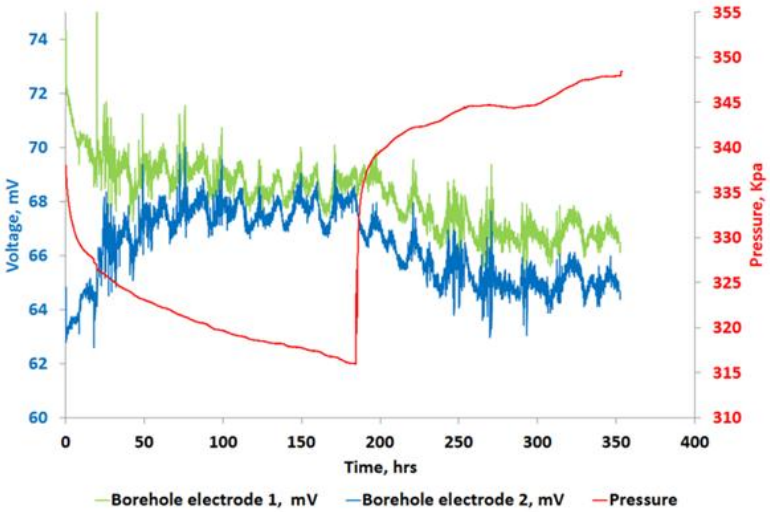

Fig. C-1 Raw voltage from PL10B BE1 and BE2 electrode. Note the cyclic temperature effect over the electrode. This cyclic effect is related to the variation of temperature in a day cycle.

The raw measurements from the PL10B borehole electrode (BE2) were manipulated for a proper curve fitting with pressure. The required manipulation did not affect the overall result. The electrokinetic raw measurements were as given in Fig. C-1. This data was treated using several methods that will be discussed in this appendix. The signal was affected by noise and temperature, as can be seen in the same figure. This noise and temperature effect in the electrode measurements made complicated the analysis of the data to determine the pressure and voltage correlation. The temperature effect has to be removed in order to determine the true values of voltage. Noise can be easily removed using a filtering utility in any signal processing software.

The first attempt to remove the temperature effect was carried using an optimisation algorithm in MATLAB® software. This optimisation algorithm is basically a mathematical expression where the voltage is in function of temperature, adding a factor (m) that will be determined by the software calculating it for the lowest variance in the results according to the original signal (fig. C-2).

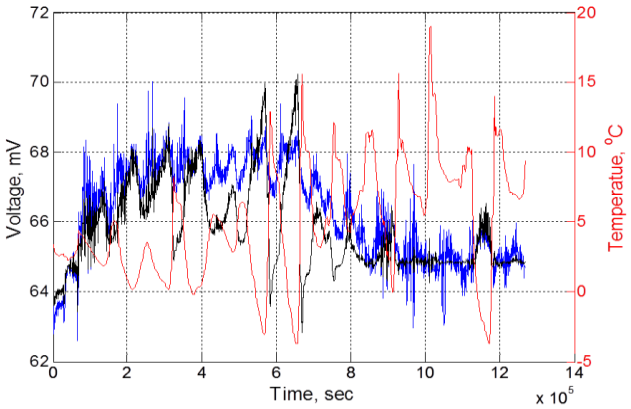

Fig. C-2 Plot of raw voltage from PL10B BE2 electrode (blue) and the optimised voltage result (black). Temperature is displayed for reference purposes (red).

The MATLAB ® program used for the optimisation stage can be seen as following:

```
function [minivar,m] =minvar(m)% Will calculate m as a function of the variance.
res=load('lab2.mat');% Will load the vectors with the temperature and voltage data.
index=326;% Pointer to closest temperature from reference value.
[minivar]= var(res.VW2-(res.VW2-res.VW2(index)).*(res.T./res.T(index)).*m);
% Function to calculate m
```

Where:

1. *lab2.mat* contains the variables for voltage and temperature arranged as a vector .
2. *minvar* is the name of the program itself, minvar(m) is stating that minvar is in fuction of factor m.
3. *m* factor is the factor which will be calculated to give the minimum variance.
4. *res.VW2* is the vector array of voltage contained in lab2.mat.
5. *index* is the pointer to the closest temperature value from the reference temperature value.
6. *res.T* is the vector array of temperature contained in lab2.mat

The MATLAB® utility *optimtool* was used to perform a loop, which consisted in several iterations until find the minimum variance and deliver the value of the *m* factor that provides that variance. For this iteration the solver *fminsearch* was used (fig. C-3).

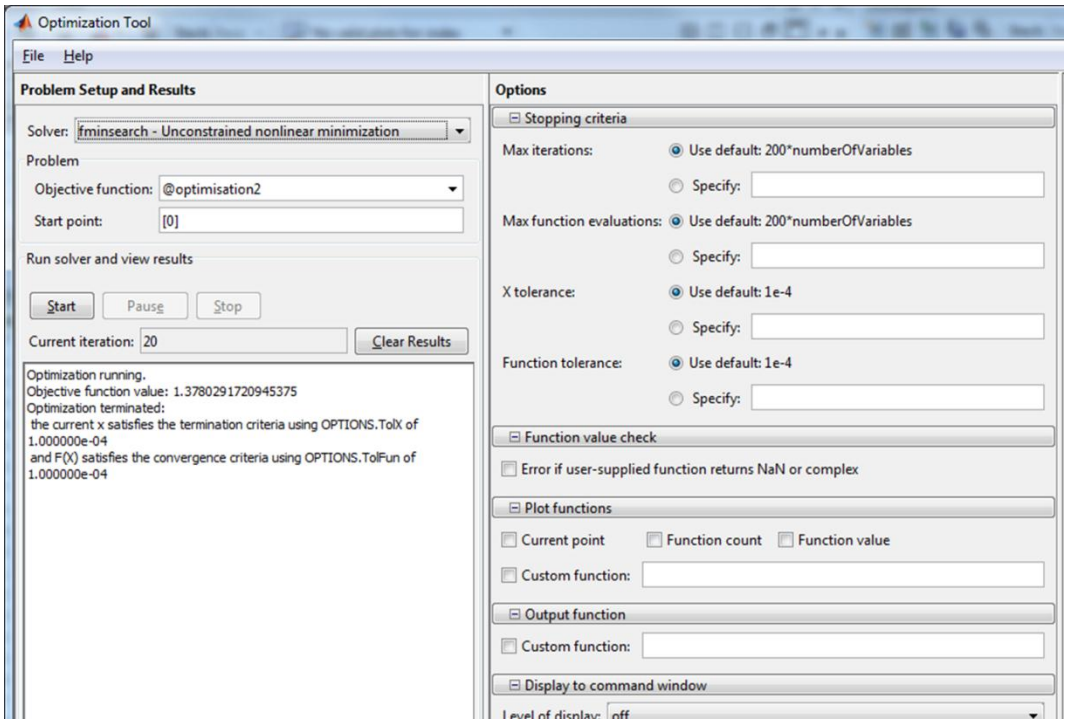

Fig. C-3 MATLAB® *optimtool* utility

The results of using the optimisation method were not successful, since no proper compensation for temperature effect was achieved. This can be seen in Fig. C-2. The results were not satisfactory since there is a miscorrelation of temperature measured and the cyclic temperature pattern in the voltage signal, derived from the different location of the temperature probe regarding the electrode position.

The following step attempted was to use fast fourier transform in MATLAB®. The process consisted in passing the measurements to a voltage gain value (dB) and then passed it to frequency domain using *fft* (fast fourier transform) utility in MATLAB®, the result of the applied method can be seen in Fig. C-4. The main frequencies cannot be properly detected. The frequencies expected were close to zero, and here two main frequencies can be identified. One of them is near to zero, the other one is yielding a very high value which could be attributed to the noise. Despite this, is not sufficiently clear to discern between frequencies needed to continue the process. Due to this, we opt for an extra procedure, which consists in applying moving averages with 25 data points (Fig. C-5) followed by a butterworth lowband pass filter (i.e. will cutoff the high frequencies). The utilities used in MATLAB® were *butter* which is used to generate the vector values for the filtering stage

and *filter* which uses these values to filter the required data (MATLAB, 2012). The syntaxis is as follows:

[b,a] = butter(n,Wn) where:

n = is the order of the lowpass band filter.
Wn = Normalised cutoff frequency
b,a = Filter coefficients.

The order (*n*) chosen for this filter was of a second order (i.e. *n=2*) assumed as the best approximation to the relationship between temperature cycle and streaming potential coefficient cycle. For the normalised frequency, the estimated frequency of the streaming potential was divided by an approximated frequency of the temperature cycle; this returned a value near to 0.006.
Freq. of streaming potential = $1/(86400 \text{ sec d}^{-1} \times 15) = 7.7 \times 10^{-7} \text{ sec d}^{-1}$
Freq. of temperature cycle = $1/(86400 \text{ sec d}^{-1}) = 1.2 \times 10^{-5} \text{ sec d}^{-1}$
$Wn = 7.7 \times 10^{-7} \text{ sec d}^{-1} / 1.2 \times 10^{-5} \text{ sec d}^{-1} = 0.06$

. The resultant voltage can be seen in Fig. C-6 plotted together with the moving averaged voltage. With this data it was possible, through a simple linear regression to obtain the results of the base, the best and the worst case, then having the error bar plot done (fig. C-7).

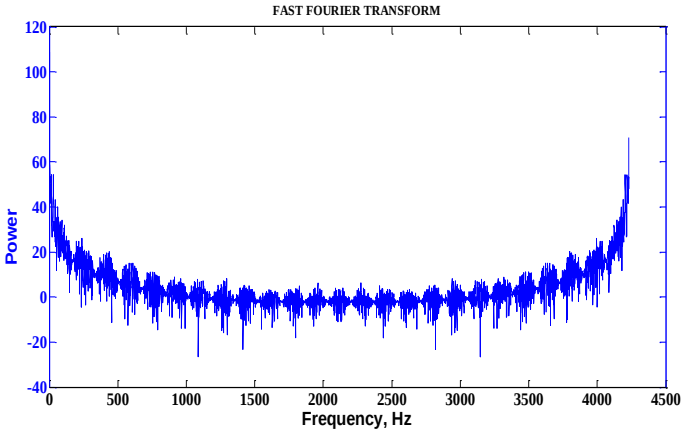

Fig. C-4 Fast Fourier Transform result.

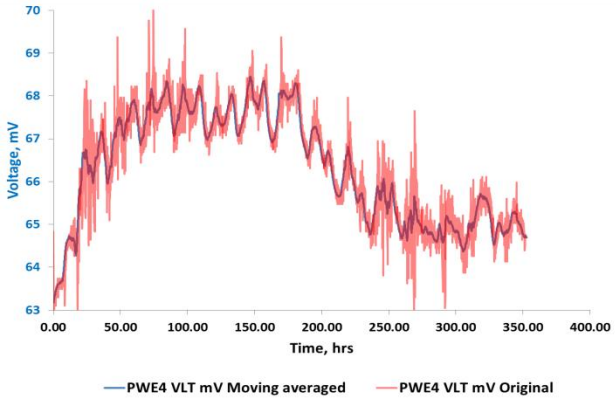

Fig. C-5 Raw (red) and moving averaged (blue) voltage from PL10B BE2 electrode.

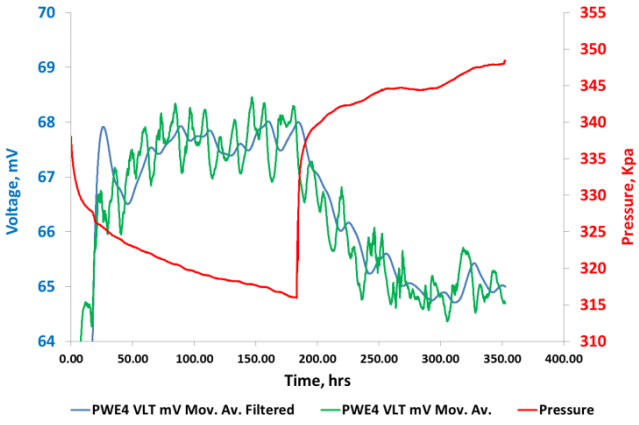

Fig. C-6 Moving averaged voltage (green) and moving averaged filtered voltage from BE2 electrode..

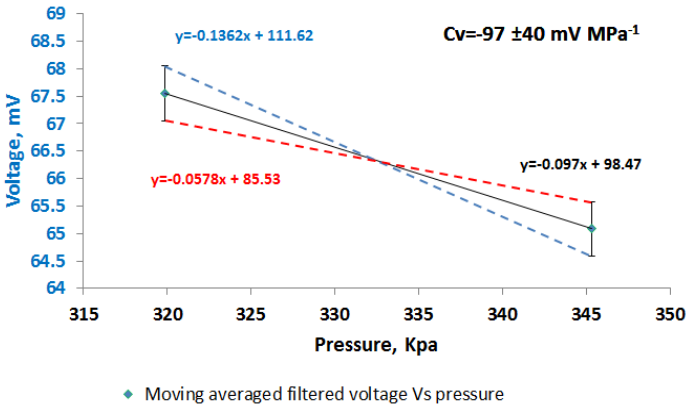

Fig. C-7 Error bar plot for coupling coefficient determination, realised with three different cases through a simple linear regression.

APPENDIX D

The molarity determination from conductivity measurements.

In order to approximate the value of mass being dissolved in the top of the boreholes (PL10A and PL10B) as part of the monitoring stage, conductivity was converted to molarity. The first step is to convert conductivity measured by the Aqua Troll 200 monitoring equipment to total dissolved solids (TDS). To reach this stage, the conductivity was multiplied by 0.64 (www.lenntech.com, 1993). Once with the data in TDS we proceed to calculate molarity in gr./L multiplying TDS by 0.000998859 (Handreck *et al*. 2005; Department of the Army, 1989). The method is proven since the plots from conductivity and molarity keep the same profiles and per Fig. D-1.

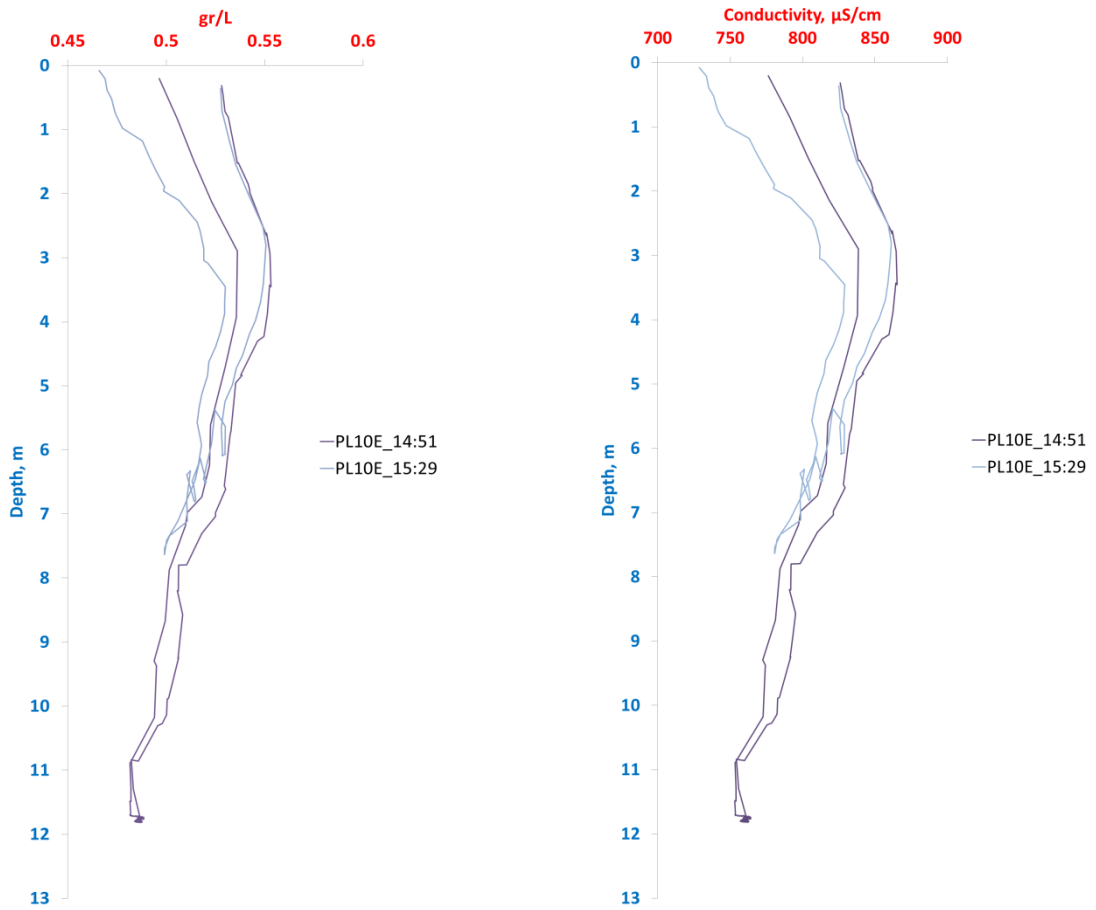

Fig. D-1 Typical conductivity and molarity profiles. The shapes are alike.

APPENDIX E

Estimation of effective permeability in chalk aquifer in BBA, Berkshire UK.

With the values of transmissivities and hydraulic conductivity, two approximations can be done. First one is with the following expression (Ritzema *et al.* 1994):

$$T_i = K_i d_i$$

Where :

T_i = Transmissivity (m^2 / day).
K_i = Horizontal hydraulic conductivty (m/day).
d_i = Thickness of the aquifer (m).

We assumed the thickness of the aquifer of 90.45 m.

In the range of the transmissivities (2049 - 2928 to 4388 m^2/day) according to Butler et al. (2009) the hydraulic conductivity is 22.6 m/day - 32.37 m/day to 48.5 m/day. Once with this values, Duggal and Soni (1996) reports an equivalency of 0.831 m/day per Darcy.

This yields values of 27.2 - 39 to 58.4 Darcys respectively. **No**te : The value declared in this work is an average of the first two values of transmissivity, reported together with the largest value (4388 m^2 / day).
Value reported :
K = 2488.5/90.45 = 27.51 m/day which is 33.2 Darcys.

Another method applied to estimate the effective permeability in the aquifer was done using the hydraulic conductivity values from Butler *et al.* (2009) data set. An average of this values was obtained, then converted to permeability:

Average value of hydraulic conductivity : 21.5 m/day
Estimation of effective permeability : 25.9 Darcys.

This result is close to the values calculated from the Jacob's method.

APPENDIX F

Cable lengths designation and locations proposed.

	READY	READY	READY	READY	READY		READY	READY	READY	READY
	1	2	3	4	5	6			7	
SE Electrodes	**L1**	**L2_Reference**	**L3**	**L4**	**L5**	**L6_Reference**	**Pb1**	**Pb2**	**Reference SE Ag *** **	**Reference SE Pb *** **
Required Length	35	80	35	35	35	80	35	35	80	80
Sensor	SE5	SEU1*	SEU2*	SE4	SE1	SE3	Pb1	Pb3	SE2	Pb2
Sensor Length	21.35	29.5	1.85	13.5	15.2	46.8	0.5	0.5	56.5	
Cable (s)	X13	XR18,X11	X3	X9	X10	X8	X4,X5	X1,X12	X7	NEW CABLE
Cable (s) length	15.7	51.9	31.5	22.3	21	30	35.5	37.5	25.5	80
Total	37.05	81.4	33.35	35.8	36.2	76.8	35.5	38	82	80
Required Length	35	80	35	35	35	80	35	35	80	80

* Depending on test results
** New sensor - Pb
*** Assuming site location for reference electrodes
**** May use SEU1 &/or SEU2 Sensors cable if any if damaged.
SE2 or reference electrode (Ag) I'm considering give it more length to the cable just in case we need to re-locate it.

	READY	READY	READY		
PWE Electrodes	**PL10E (Water table 16m BGL) Permanent electrode**	**PL10B (Water Table 19m BGL) Permanent electrode**	**Travelling Electrode (Calculated at water table 16m BGL)**		
Required Length	52	52	52		
Sensor	WE300/5	WE300/2	WE300/6		
Cable assign to new sensor (Pb)					
Sensor Length	26	26.5	46.5		
Cable connection above water table					
Cable (s)	X6,X14	XR16,X15	XR17,X2		
Cable (s) length	37.8	38.9	46		
Total	63.8	65.4	92.5		
Required Length	65	65	90		

*Water table 16m Depth.
*Sensor should be 20m under water && TBC

	No usable
	Assigned sensor
	Free sensor-to be used
	Cable not assigned

PWE Sensor	Cable length	
WE300/1	23.5	FREE
WE300/2	26.5	
WE300/3	23.5	FREE
WE300/4	21.5	
WE300/5	26	
WE300/6	46.5	
WE300/7	7.5	
WE300/8	9.2	
WE300/9	2.1	
WE300/10	1	

SE Sensor	Length	Condition
SEU1	29.5m	&&
SEU2	1.85m	&&
SE1	15.2m	Ok
SE2	56.5m	Ok
SE3	46.8m	Ok
SE4	13.5m	Ok
SE5	21.35m	OK

ID	Qty	Length
X1	1	20
X2	1	26
X3	1	31.5
X4	1	17.5
X5	1	18
X6	1	27.4
X7	1	25.5
X8	1	30
X9	1	22.3
X10	1	21
X11	1	15.5
X12	1	17.5
X13	1	15.7
X14	1	10.4
X15	1	10.4
X16	1	4.2
XR16	Reel 1	28.5
XR17	Reel2	20
XR18	Reel 3	36.4
		397.8
		597.8 Total
		185.7
		783.5 Overall total

Fig. F-1 Aerial view of the site and proposed sensor location.